Mafic-ultramafic intrusions of Matokulma, Palojärvi, and Hongonniittu within the Central Finland Granitoid Complex with special reference to their petrogenesis and ore potential

Seppo Karvinen[1]*, Hannu V. Makkonen[2], Perttu Mikkola[3], O. Tapani Rämö[1], Hannu Huhma[4], Matti Niskanen[3]

[1]*University of Helsinki, Department of Geosciences and Geography, Gustaf Hällströmin katu 2, 00014 University of Helsinki, Finland*
[2]*Suomen Malmitutkimus Oy, Taivaanpankontie 1 B 40, 70200 Kuopio, Finland*
[3]*Geological Survey of Finland, Viestikatu 7, 70211 Kuopio, Finland*
[4]*Geological Survey of Finland, Vuorimiehentie 5, 02151 Espoo, Finland*

VERTAISARVIOITU
KOLLEGIALT GRANSKAD
PEER-REVIEWED
www.tsv.fi/tunnus

Abstract

We describe three previously unknown or poorly studied mafic-ultramafic intrusions (Matokulma, Palojärvi, Hongonniittu) from the south-central part of the Paleoproterozoic Central Finland Granitoid Complex (CFGC). The ore potential and petrogenesis of the intrusions, with the focus on Matokulma and Palojärvi, are discussed based on petrography and geochemistry and, possible relationships with the Ni-Cu ore potential Vammala–Kotalahti type intrusions are examined. The poorly exposed Hongonniittu intrusion is likely genetically related to the Palojärvi intrusion. Median Mg-numbers for Matokulma and Palojärvi are 72 and 49, respectively. They consist of cumulus clinopyroxene, orthopyroxene and plagioclase, in case of Palojärvi also Fe-Ti oxide, and oikocrystic magmatic amphibole enclosing the cumulus phases. In Matokulma, mafic dikes cut the surrounding granitoids. A late leucogabbro dike with a U-Pb zircon age of 1882 ± 5 Ma constrains the minimum age for the Palojärvi intrusion. The Palojärvi leucogabbro has relatively radiogenic Nd isotope composition and is, in this respect, similar to Kotalahti-type mafic-ultramafic intrusions farther northeast. The parental magmas of the Matokulma and Palojärvi intrusions contained approximately 4–6 wt.% and 2–4 wt.% MgO, respectively. Magmatic amphibole, enrichment in large ion lithophile elements (LILE) and depletion in high field strength elements (HFSE) indicate crystallization from hydrous, evolved basaltic magmas. Owing to their evolved nature, the intrusions are not potential for magmatic Ni-Cu mineralizations, but Palojärvi could potentially host a Fe-Ti-V mineralization in deeper, concealed parts of the intrusion.

Keywords: gabbro, ore potential, Svecofennian, Central Finland Granitoid Complex, Paleoproterozoic, geochemistry, age determination, petrogenesis

*Corresponding author (email: seppo.karvinen@helsinki.fi)

Editorial handling: Shenghong Yang (email: shenghong.yang@oulu.fi)

1. Introduction

During the last eighty years, more than ten variably sized magmatic Ni-Cu deposits have been exploited in southern and central Finland and the ore formation model for these deposits is well constrained (e.g., Makkonen 2015; Makkonen et al. 2017). They are hosted by ultramafic–mafic intrusions, or their immediate country rocks, and were formed by segregation of sulphide melt triggered by assimilation of sulphide-rich country rocks, most typically migmatized paragneisses (Peltonen 2005; Makkonen 2015).

The deposits are found in two separate belts: the Kotalahti Ni belt along the Archaean–Proterozoic boundary and the Vammala Ni belt along the southern edge of the Central Finland Granitoid Complex (CFGC, Fig. 1). The host intrusions are of similar age (1880–1890 Ma) but display certain differences in occurrence type and chemical composition, attributed to varying geotectonic settings. The intrusions of the Vammala belt, which are typically ultramafic and lack distinct layering, have been interpreted as magma conduits (Peltonen 1995a; 1995b). The intrusions in the Kotalahti belt usually include both mafic and ultramafic lithologic units and display layered structures. Mafic to ultramafic intrusions coeval with those of the Kotalahti and Vammala belts are also known within the CFGC, but no significant Ni-Cu mineralizations are known. Instead, they have potential for economic ilmenite mineralizations (e.g., Peltonen 2005).

In this study, we present field, petrographical, geochemical, and isotope data from three separate mafic intrusions located in the southern part of the CFGC (Fig. 1). Prior to this study, only one of the intrusions (Palojärvi) was briefly evaluated for its Ti-Fe potential (Akiander 1972), the two other intrusions, Hongonniittu and Matokulma, are new findings. The data will be used to interpret parental magma compositions and petrogenesis of the intrusions. The geological environment of these intrusions conform to that of the Vammala belt, as they intrude within or in the vicinity of migmatitic paragneisses. This paper stems from the Master's thesis of the first author (Karvinen 2019).

2. Geological setting

The studied intrusions are located in southern part of the CFGC (Fig. 1 and 2). The bedrock in the area is dominated by calc-alkaline granitoids, which based on results from surrounding areas (e.g., Nironen 1989; Nikkilä et al. 2016) and the authors' unpublished data, are mainly 1885–1880 Ma old. South of the study area CFGC is separated from the paragneisses of the Pirkanmaa migmatite belt by a narrow discontinuous belt of volcanic rocks with calc-alkaline, arc-type geochemical signature and crystallization ages similar to those of the granitoids north of them (Kähkönen 1989; Heikura 2017; Mikkola et al. 2018a). The granitoids and volcanic units have been interpreted as having been formed in an active continental magmatic arc setting (e.g., Nironen 2017; Mikkola et al. 2018b).

Based on their maximum deposition age and geological relationship to other units, the protoliths of the Pirkanmaa migmatite suite were deposited along a passive continental margin close to 1.91 Ga (Claesson et al. 1993; Lahtinen et al. 2017), briefly before the onset of subduction related magmatism in the area. Smaller paragneiss areas are found within the study area and have been coined the "Vilppula suite" (Bedrock map of Finland – DigiKP), purely on geographical base as no age or geochemical data are available.

In addition to the studied intrusions, other mafic to ultramafic intrusions exist in their vicinity (Fig. 2). These intrusions consist mainly of gabbros which have gradual contacts with the dioritic and ultramafic components (Laiti 1976; Sjöblom 1990). These intrusions have not been studied in detail and based on their location have been regarded as mafic members of the CFGC (Bedrock map of Finland – DigiKP).

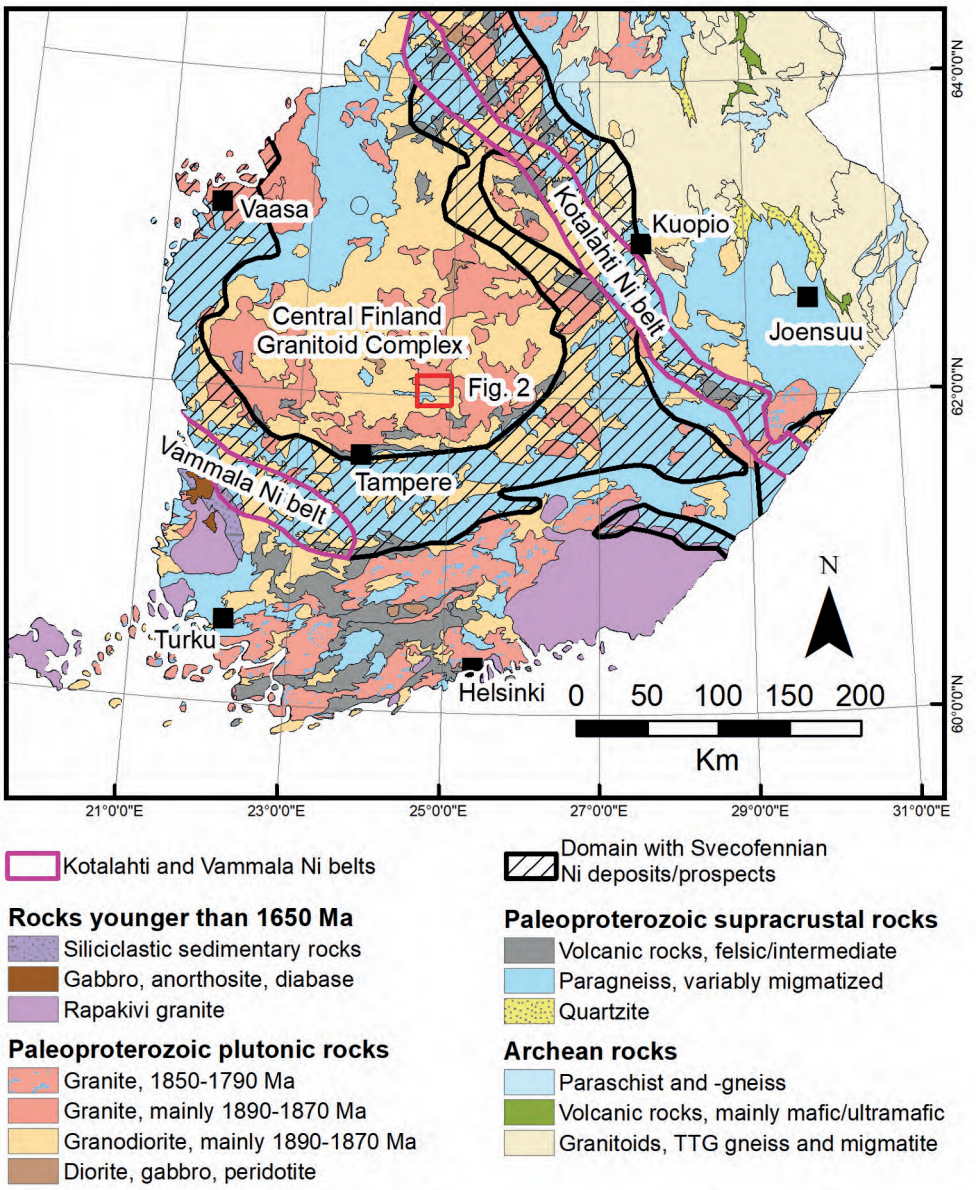

Figure 1. Bedrock map of southern and central Finland showing location of the study area and the Vammala and Kotalahti belts hosting the known economic Ni-Cu deposits. Bedrock map modified from Nironen et al. (2016). Domain with Svecofennian Ni deposits/prospects and Kotalahti/Vammala Ni belts is from Makkonen (2015).

3. Methods and materials

The intrusions were mapped by GTK's regional ore potential evaluation project. For this study, 62 outcrop samples were analysed in Labtium Ltd (now Eurofins Labtium Ltd) for whole-rock composition. XRF-method was used for the main elements and certain trace elements (Labtium methods 175X and 176X). Comprehensive trace element analysis of 21 samples were conducted using Inductively Coupled Plasma-Optical Emission Spectrometry (ICP-OES, Labtium

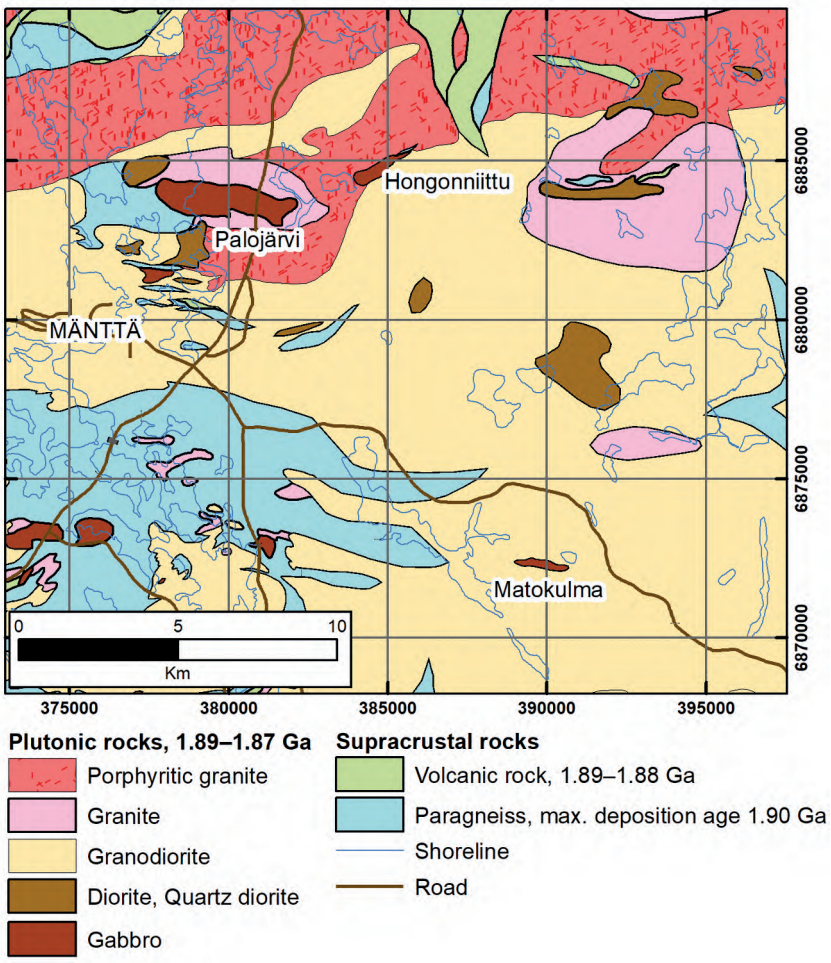

Figure 2. Bedrock map of the study area modified from Bedrock map of Finland – DigiKP. Basemap © National Land Survey of Finland.

method 308M) and Inductively Coupled Plasma-Mass Spectrometry (ICP-MS) (Labtium method 308P). Platinum group elements were analysed using ICP-OES (Labtium method 705P). For detailed description of the applied methods see Rasilainen et al. (2007). The analyzed elements and respective detection limits are reported in Electronic Appendix C.

Mineral compositions were determined in GTK's Espoo laboratory using a Cameca SX100 electron microprobe. In silicate analysis acceleration voltage was 15 kV, beam current 20 nA, and beam diameter 5 µm, for oxide analysis beam current was 40 nA and beam diameter 1 µm. Amphibole analyses were classified according to the current IMA classification scheme (Hawthorne et al. 2012) using the spreadsheet of Locock (2014). Additional analytical information can be found in Electronic Appendix C.

Crushing, separation, sample bead preparation and analyses for single grain zircon age determinations were done in GTK's Espoo laboratory. Analyses were performed with a Nu Plasma AttoM single collector ICP-MS connected to a Photon Machine Excite laser ablation system. Detailed description of the analytical method can be found in Molnár et al. (2018). Results can be found in Electronic Appendix A.

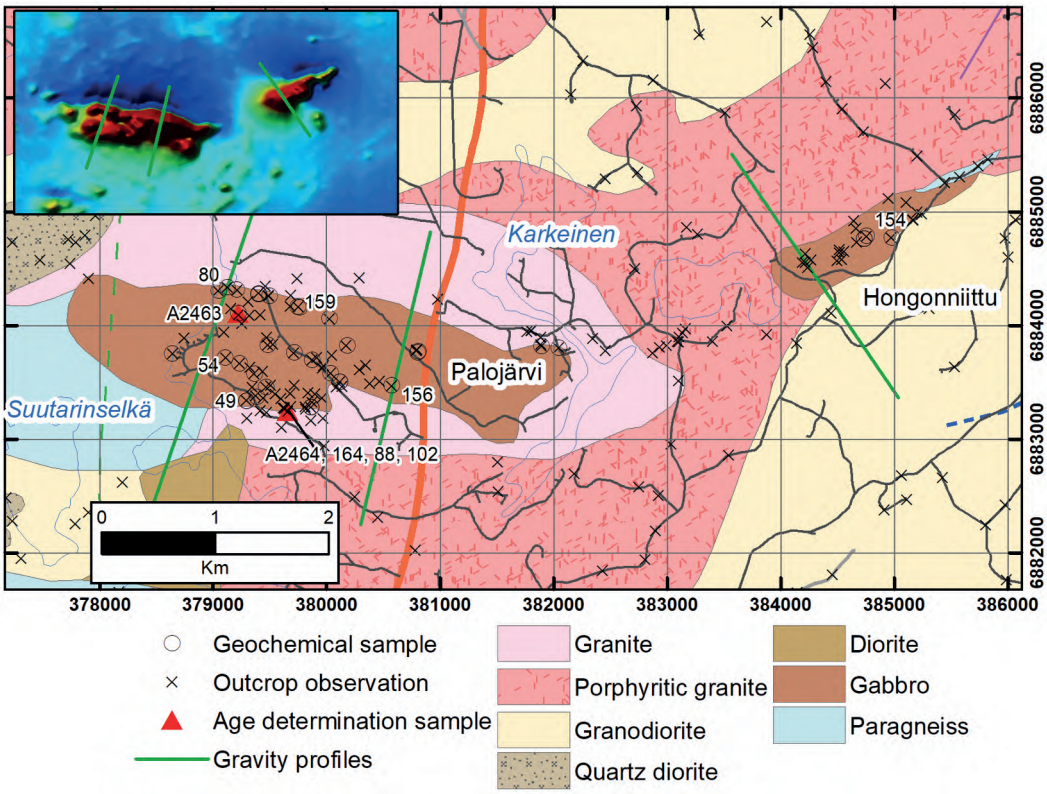

Figure 3. Geological map of the Palojärvi and Hongonniittu intrusions displaying sample and observation sites. SIKA-2017- has been omitted from the site numbers for brevity. Map modified from Bedrock map of Finland - DigiKP. In inset aeromagnetic map of the same area, red indicates high and blue low values. Green lines indicate the gravity measurement lines

Sm-Nd isotope compositions were analysed from whole-rock samples using Nu instruments multi-collector inductively coupled plasma mass spectrometer (MC-ICP-MS) in GTK's laboratory in Espoo. Description of the analytical method can be found in the Electronic Appendix C.

Five ground gravity profiles were measured across the intrusions, two for Palojärvi (total length 3300 m), one for Hongonniittu (2640 m), and two for Matokulma (3250 m). Point separation was 40 meters. Measurements were done with Scintrex CG-5 autograv and levelling were done with Leva hose scale. The measurements are tied to the Geodetic Institute's 1st class Finnish national gravity point network. To constrain the parameters for modelling the depth of the intrusions, density and susceptibility of all outcrop samples were measured in GTK's petrophysical laboratory in Kuopio.

4. Results

4.1. Field observations

4.1.1. Palojärvi and Hongonniittu

In Palojärvi area the two closely spaced intrusions, clearly visible on the aeromagnetic map (Fig. 3), are referred to as Palojärvi and Hongonniittu.

Palojärvi is elongated, EW-striking and approximately 3.4 km x 0.9 km in surface section (Fig. 3). The most common rock type of the intrusion is a porphyritic gabbro, the more amphibole rich rocks can be classified as ultramafic (hornblendites). In leucocratic gabbros, plagioclase is more abundant and, in some samples, present as phenocrysts (Fig. 4d). The rocks are dark gray to greenish gray, middle to coarse-grained. Dark green

Figure 4. a) Granite dike (white arrow) hosting mafic enclaves and intruding into the layered gabbro of the Palojärvi intrusion. Observation point SIKA-2017-88. b) Close-up of a), showing the gradational layering from more mafic to leucocratic. c) Dark and dark green round crystals of amphibole and weathered brown crystals of orthopyroxene, visible as rust-colored dents on the surface of the outcrop. Hornblende norite, observation point SIKA-2017-80. d) Porphyric plagioclase (light) and interstitial hornblende (dark green). Porphyric gabbro, observation point SIKA-2017-159. Length of the compass (visible in a) is 12 cm, diameter of the coin is 2.6 cm.

to black amphibole crystals are often 1–2 cm, locally up to 4 cm in diameter. Besides amphibole and plagioclase, pyroxene and biotite are major phases in some samples. Magnetite is a common accessory phase, pyrite is occasionally present.

Compositional layering is visible on one outcrop near the southern margin of the intrusion, where steeply NW dipping layering is formed by gradational changes in the proportions of amphibole and plagioclase. The layered sequence is crosscut by granitoid dikes with mafic enclaves (Fig. 4a).

A leucocratic gabbro dike sampled for geochronology crosscuts melagabbro in the NW part of the intrusion (A2463). Felsic veins and dikes crosscut the mafic rocks on several outcrops. These medium-grained granite dikes locally contain garnet as well as mafic enclaves.

The wall rock of the intrusion is a quartz-rich granite, which is light to pink in color and strongly foliated. Both biotite and amphibole are present in small amounts. The marginal zone along the southern contact of the intrusion is gneissose (Fig. 5a). Mingling textures between granite and the mafic rocks are present near intrusions contacts (Fig. 5).

Hongonniittu is a SW trending intrusion with limited exposure which, based on aeromagnetic data, is 2.0 x 0.5 km in area. Because of limited number of outcrops, mapping and sampling focused on the Palojärvi; but based on field observations and thin sections, Hongonniittu and Palojärvi are similar.

Figure 5. Mingling and mixing textures in the Palojärvi intrusion. a) Elongated mafic enclaves with felsic interstitial material. b) Magmatic breccia with angular and semi-rounded blocks of mafic rock within felsic rock. c) Irregular mafic enclave with core-mantle gradation, with a more plagioclase-rich mantle (cooling structure?). d) Complex mingling textures of more leucocratic material within mafic-ultramafic host. Observation points SIKA-2017-164 (a), -49 (b, d), -102 (c). Length of the compass is 12 cm, diameter of the coin is 2.6 cm.

4.1.2. Matokulma

The Matokulma intrusion is roughly EW oriented, elliptical body 1.7 km by 0.3 km in surface section (Fig. 6.) It is composed of melagabbros with white to pink plagioclase and black to dark green (phenocrystic) amphibole. The amount of plagioclase typically varies within a scale of tens of centimetres causing variation in the modal composition from gabbroic to hornblenditic.

Steep SWW-dipping compositional layering was observed on one outcrop (SIKA-2017-6) near the east contact of the intrusion, caused by alternating 5 to 20 cm thick layers of fine-grained ultramafic rock and medium-grained gabbro (Fig. 7a, b).

The main wall rock of the Matokulma intrusion is a garnet-bearing tonalite and locally paragneiss. Pink granite is found locally south of the western and central parts of the intrusion, where granite

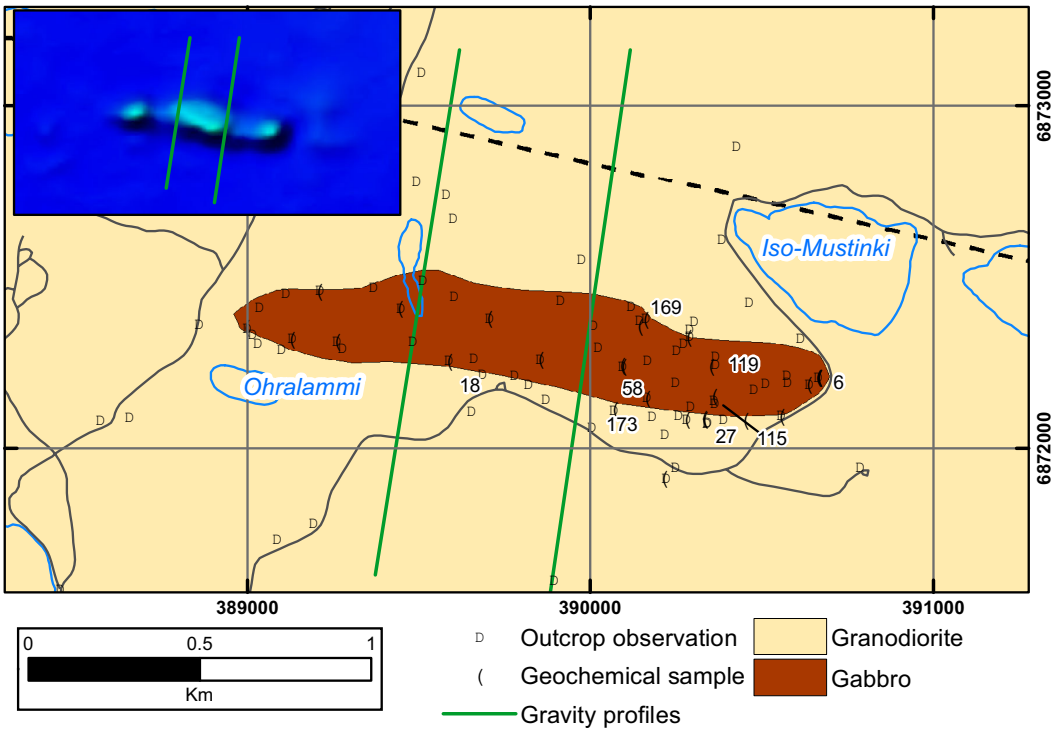

Figure 6. Geological map of the Matokulma intrusion displaying sample and observation sites, country rock (granodiorite) according to GTK's DigiKP bedrock map. SIKA-2017- has been omitted from the site numbers. In inset aeromagnetic map of the same area, green indicates higher and blue lower values. Green lines indicate the gravity measurement lines. Basemap ©National Land Survey of Finland.

and gabbro display mingling textures (Fig. 7c, d). Further away from the contact the granite is medium grained and pink, grading to white and finer-grained closer to the contact. Contact zone featuring paragneiss with garnet porphyroblasts and gabbro is exposed on outcrop SIKA-2017-27 along the SE margin of the intrusion. Between the garnet-paragneiss and the gabbro intrusion is a mixed rock, composed of coarse green amphibole, white plagioclase, quartz, and epidote. A similar mixed rock is exposed on outcrop SIKA-2017-18.

Both the tonalitic country rock (Fig. 7e, f) and the gabbro are cut by mafic dikes (0.2 to 1.5 m in width) which dip steeply (70–80°) to north (350-010). These gray, fine-grained and sheared dikes are found close to intrusion contacts. Some of the dikes are cut by leucocratic veins. Besides the mafic dikes, the gabbro is also sporadically intruded by quartz-feldspar veins and aplite dikes.

4.2. Petrography

4.2.1. Palojärvi

The mafic-ultramafic rocks of the Palojärvi intrusion display cumulus textures, with chadacrysts of plagioclase ± orthopyroxene ± clinopyroxene ± Fe-Ti oxides ± olivine as the cumulus phases, typically enclosed in large amphibole oikocrysts, which is the most abundant mineral in most samples (Fig. 8). The oikocrystic amphibole is often partly replaced by secondary amphibole (hornblende or actinolite). Oikocrystic amphibole and orthopyroxene are also replaced by acicular to fibrous light brown clinoamphibole, likely cummingtonite (Fig. 8c, d). Biotite is a common minor phase, often chloritized and in some samples occurring as a poikilitic phase enclosing plagioclase chadacrysts.

Figure 7. Matokulma outcrop pictures. a) and b) Layering displayed by variation in the modal amount of plagioclase (white) and hornblende (green) and grain size, outcrop SIKA-2017-6. c) and d) Mingling textures between granite and gabbro on outcrop SIKA-2017-115, notice that the granite is more leucocratic near the contact to the gabbro. e) Mafic dike intruding garnet tonalite country rock of the intrusion, outcrop SIKA-2017-169. f) Stoped, rounded fragments of the garnet tonalite are found in the dike, outcrop SIKA-2017-169. Length of the compass is 12 cm, diameter of the coin is 2.6 cm.

Olivine is present in only one sample (olivine-hornblende-norite, SIKA-2017-80.1) where subhedral chadacrysts of olivine and resorbed plagioclase are enclosed in amphibole, orthopyroxene, and phlogopite oikocrysts (Fig. 8). There is a symplectite texture between amphibole or pyroxene and plagioclase (Fig. 8a, b). Some of the olivine is completely oxidized to magnetite.

Fe-Ti oxides, mainly magnetite, with or without ilmenite lamellae, are present in virtually all samples. Discrete grains of ilmenite are also present in some samples. The mineral habits vary from euhedral grains, grain aggregates to amoeba-like exsolutions from mafic minerals. Dark green spinel (hercynite) is present in the most amphibole-rich samples. Apatite is the second most common accessory phase, typically occurring as euhedral prisms. Chromite, zircon, quartz, and sulphides are less common. Pyrite and chalcopyrite are present as small anhedral grains together with oxides or mafic silicates.

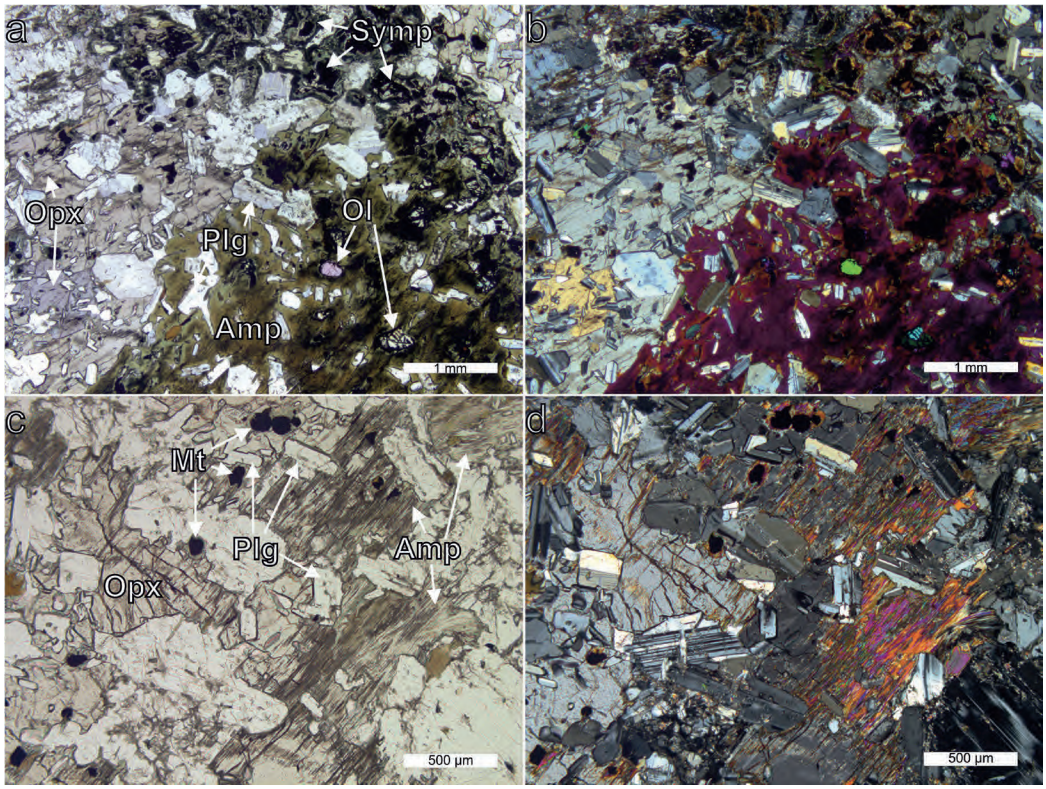

Figure 8. Optical microscope pictures of olivine-hornblende-norite (sample SIKA-2017-80.1, Palojärvi). Oikocrystic amphibole (amp) and orthopyroxene (opx) enclosing cumulus plagioclase (plg) and olivine (ol). Olivine is often oxidized to magnetite. Notice the symplectites (Symp; a, b), where olivine is surrounded by orthopyroxene and a reaction rim against plagioclase. c, d) Secondary acicular amphibole with orange-red interference colors is replacing orthopyroxene. a) and c) are in plane-polarized light, b) and d) in cross-polarized light.

4.4.2. Matokulma

The mafic-ultramafic rock types in Matokulma are similar to those in Palojärvi with most samples displaying cumulus textures with plagioclase ± clinopyroxene ± orthopyroxene enclosed in oikocrystic amphibole. Accessory phases include apatite, chromite, and Fe-Ti oxides. Sulphides (pyrite and pyrrhotite) are rare. Amphibole is found even in the most primitive samples, where it encloses euhedral orthopyroxene and clinopyroxene (Fig. 9). Based on the primitive samples with well-preserved cumulus pyroxenes within the poikilitic amphibole, the amphibole is interpreted as magmatic. Phlogopite partially, to completely, altered to chlorite is another hydrous phase found in the most primitive samples in Matokulma.

Clinopyroxene is the dominant pyroxene, often showing an alteration rim in contact with the poikilitic amphibole, 'bubbly' interior textures, and resorbed grain boundaries (Fig. 9). Pyroxene is completely altered in some samples, in which only round pseudomorphic actinolite grains are present. In the same samples, the oikocrystic amphibole is also replaced by a secondary amphibole. In some cases, the oikocrystic amphibole is replaced by biotite which can be further altered to chlorite. Orthopyroxene is a rare cumulus phase, present as euhedral crystals with rust brown alteration in sample SIKA-2017-115.2 (Fig. 9a, b). In sample SIKA-2017-173.1 (Fig. 9c, d), orthopyroxene is found both as a poikilitic phase together with amphibole enclosing cumulus clinopyroxene and as a cumulus phase within amphibole. Acicular

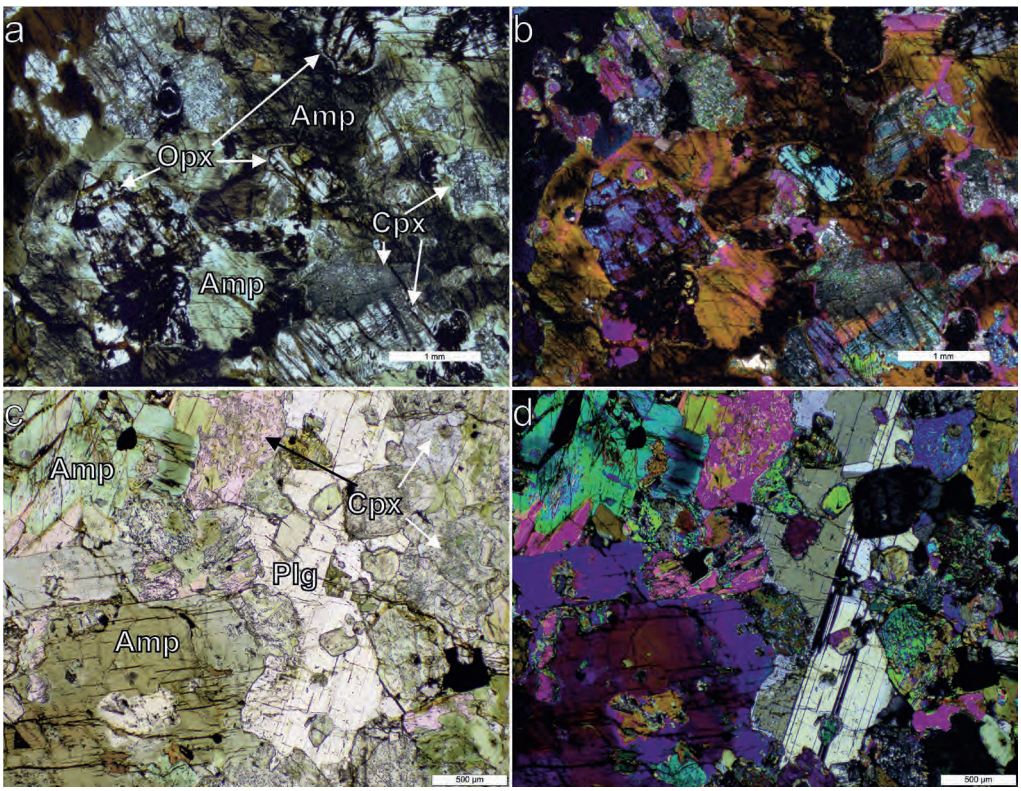

Figure 9. Optical microscope pictures of representative mafic-ultramafic rocks from the Matokulma intrusion. Oikocrystic amphibole (Amp) encloses euhedral cumulus orthopyroxene (Opx) and clinopyroxene (Cpx). Oikocrystic, interstitial plagioclase (Plg). a) and c) are in plane-polarized light, b) and d) in cross-polarized light. Hornblende gabbro (a, b; sample SIKA-2017-115.2) and plagioclase-bearing pyroxene hornblendite (c, d; sample SIKA-2017-173.1). Notice that the thin section in a, b) is too thick, resulting in 2nd order interference colors in orthopyroxene.

serpentine pseudomorphs after orthopyroxene are present in some samples.

Cumulus plagioclase is common in all but the most primitive samples, where it is found as a rare intercumulus phase enclosing pyroxenes (Fig. 9c, d). Plagioclase is often partially sericitized or pigmented and, in many samples, completely altered.

Dike rocks

The fine grained and sheared dike rocks are generally more altered than the Matokulma gabbros. The groundmass consists of sericitized plagioclase, pleochroic light to dark green amphibole, brown biotite or chlorite, and varying amounts of quartz and opaque minerals. Amphibole is present as coarse-grained groups or as elongated fine-grained crystals. Quartz is present as elongated grain aggregates parallel to the foliation. Sample SIKA-2017-58.1 is a relatively unaltered dike rock with magmatic mineral paragenesis and grain size similar to the gabbros. Primary clinopyroxene and orthopyroxene crystals are present in roughly equal proportions as phenocrysts in a matrix of prismatic plagioclase. The pyroxenes are partly or completely mantled by dark green pleochroic amphibole. Pyroxenes often occur as glomeroporphyric groups. Clinopyroxene displays possible exsolution textures and growth zonation, and there is a reaction rim in contact with plagioclase. Apatite, chromite, and magnetite are present as accessory phases, often in contact or as inclusions in mafic phases.

4.3. Mineral chemistry

The mineral chemistry presented in this section focuses on the ferromagnesian phases (pyroxenes, amphiboles), used in parental magma composition calculations as well as in petrogenetic and ore potential discussion. The mineral chemical data are found in Electronic Appendix A.

Olivine ($Fo_{42–49}$, ≤250 ppm Ni), is present only in one of the samples from Palojärvi as a subhedral cumulus phase (Fig. 8) that is often completely oxidized to magnetite.

4.3.1. Pyroxenes

Pyroxene compositions are presented in Fig. 10. Palojärvi orthopyroxene compositions range from enstatites to ferrosilites. The median ternary composition is $En_{52}Fs_{45}Wo_{2,}$ variations for end member proportions being $En_{41–59}$, $Fs_{39–55}$, and Wo ≤3 %. Mg# ranges from 44 to 61, with a median of 54. The poikilitic orthopyroxene oikocrysts in sample SIKA-2017-80.1 have the highest Mg# (median 58). Nickel and Cr median contents are low, 45 ppm and 70 ppm, respectively. Al_2O_3 concentrations range from 0.65 to 1.93 wt.%, with a median of 1.1 wt.%. The highest values are also found in sample SIKA-2017-80.1.

Orthopyroxene in the Matokulma samples are enstatites ($En_{65–74}$) with a median composition of $En_{69}Fs_{29}Wo_3$. Alumina concentration ranges from 0.4 to 2.1 wt.% and correlates positively with TiO_2. Nickel concentration is low (median 50 ppm Ni). Generally, the most magnesian orthopyroxenes have the highest Cr concentration, up to 1180 ppm in SIKA-2017-115.2. Clinopyroxene, present in three samples from Palojärvi, has a median composition of Mg# = 69, $En_{38}Fs_{17}Wo_{45}$ and Cr and Ni concentrations of 80 and 20 ppm, respectively. The clinopyroxene in sample SIKA-2017-156.1 is present as round phenocrysts up to 3 mm in diameter, mantled by dark green amphibole. The clinopyroxene in this sample is anomalous not only in habit and texture but also for its relatively magnesian (Mg# = 75) composition and enrichment in Al_2O_3 (3.0–5.5 wt.%), Cr (median 1300 ppm), Ni (median 120 ppm) TiO_2 (0.5–0.9 wt.%), and V (740–1700 ppm).

Clinopyroxene is more common than orthopyroxene in the Matokulma intrusion. Clinopyroxene is generally diopside, with a median composition of $En_{42}Fs_{12}Wo_{46}$. Clinopyroxene Mg# has a limited variation from 77 to 83 between samples. TiO_2 and Al_2O_3 content correlate positively and have median concentrations of 0.29 and 0.39 wt.%, respectively. Chromium content is 720 ppm in median, maximum being 3000 ppm. Nickel content is low, from below detection limit to 150 ppm in maximum and 20 ppm in median. In sample SIKA-2017-173.1 most grains have elevated concentrations (2–3 wt.% Al_2O_3 and 0.2–0.5 wt.% TiO_2) and also higher Cr and V (up to 3000 ppm, 3800 ppm, respectively) and Mg# (83).

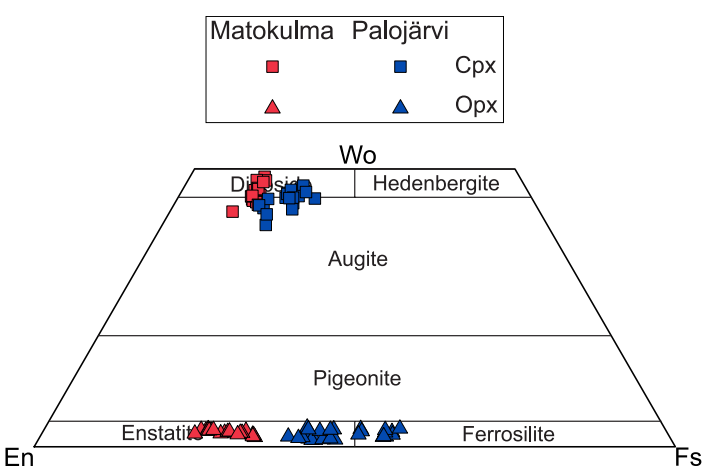

Figure 10. Pyroxene compositions from Matokulma (red symbols) and Palojärvi (blue symbols) intrusion plotted into the pyroxene quadrilateral of Morimoto et al. (1988). Matokulma pyroxene are more magnesian (higher En content) than Palojärvi pyroxenes.

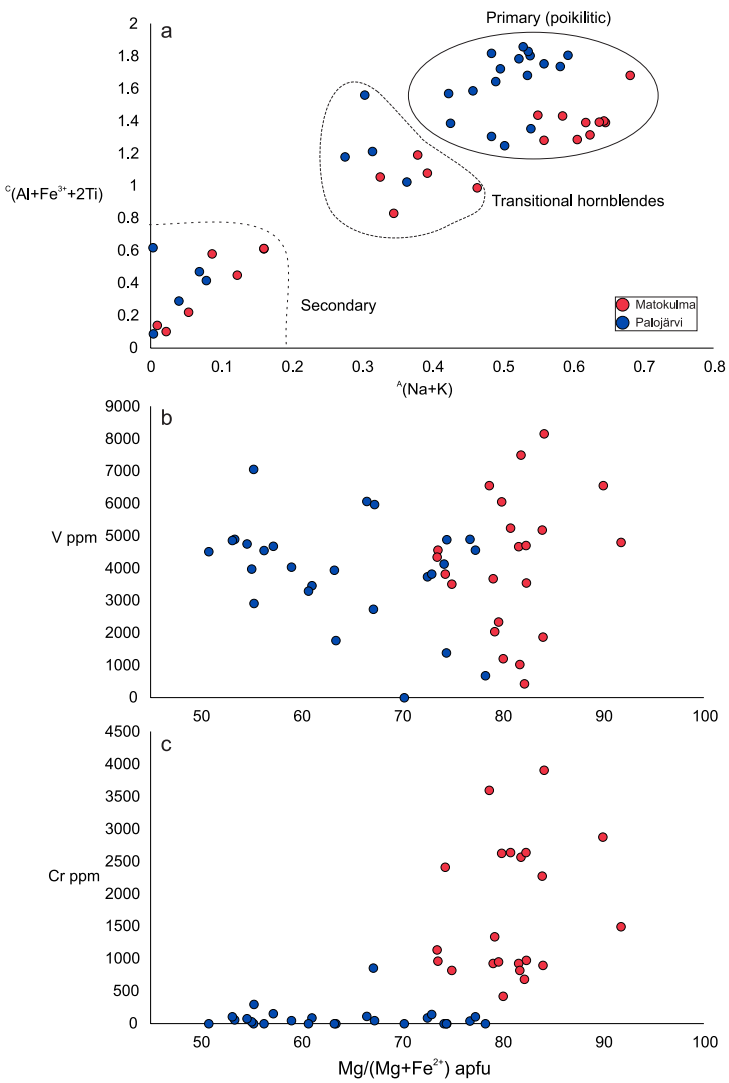

Figure 11. Amphibole mineral chemistry. a) Na+K atoms in amphibole's structural A site vs Al+Fe^{3+}+2Ti atoms in the structural C site. Magnesium number (Mg/(Mg+Fe^{2+}) atoms per formula unit (apfu)) versus V (b) and Cr (c). Matokulma samples have higher Mg# and are enriched in Cr compared to Palojärvi. Red circles are Matokulma analyses, blue circles are Palojärvi samples.

4.3.2 Amphiboles

Large oikocrystic amphiboles belong mainly to the Ca-amphibole subgroup (Hawthorne et al. 2012) and they were classified primarily as magnesio-hastingsites, pargasites, magnesio-hornblendes or magnesio-ferrihornblendes. Primary amphiboles have ^{A}(Al+Fe^{3+}+2Ti) > 1.2 and ^{C}(Na+K+2Ca) > 0.5 (Fig. 11a), where the values are the cations occupying A and C sites in the amphibole structure. Secondary amphiboles (actinolite, cummingtonite) have ^{A}(Al+Fe^{3+}+2Ti) < 0.8 and ^{C}(Na+K+2Ca) < 0.2 (Fig. 11a). Actinolite typically replaces both cumulus pyroxene and poikilitic amphibole in strongly altered samples. In Palojärvi, acicular cummingtonite replaces orthopyroxene in some samples (Fig. 8c, d).

Amphibole in Palojärvi is more enriched in Ti and Fe^{3+} (calculated), with some amphiboles classified as Ti-rich magnesio-hastingsites and hornblendes, typically as magnesio-ferri-hornblendes. Primary Matokulma amphibole has high Mg# (>80) and contains substantial Cr (1000–4000 ppm) whereas in Palojärvi, the amphibole is more depleted (>200 ppm Cr), except one actinolite outlier in sample SIKA-2017-156.1 with 860 ppm Cr (Fig. 11c).

4.3.3. Oxides

Magnetite and ilmenite, abundant in Palojärvi, were analyzed from two samples. In sample SIKA-2017-88.2, the magnetite is vanadiferous, containing up to 1.37 wt.% V_2O_3 and 0.29–0.54 wt.% TiO_2, whereas ilmenite contains 0.12–0.17 wt.% V_2O_3. In sample SIKA-2017-156.1, magnetite and ilmenite contain 0.95 and 0.20 wt.% of V_2O_3, respectively. The magnetite contains 0.05 wt.% of TiO_2.

4.4. Whole-rock chemistry

The average compositions of the intrusions and dikes are in Table 1 and all analytical data can be found in Electronic Appendix A.

4.4.1. Palojärvi

Palojärvi intrusion has a median SiO_2 of 45.3 wt.% with a large variation from 39.1 to 52 wt.% (Fig. 12a). Concentration of MgO is generally low but it also shows high variability (2.12–14.15 wt.%), as does Mg# (32–66), with highest values observed from altered hornblendites. Al_2O_3 and FeOt vary from 10.4 to 27.5 wt.% and from 6.7 to 20.9 wt.%, respectively. Strontium has negative correlation with MgO and positive correlation with Al_2O_3, indicating that plagioclase is the main host of Sr. The concentrations of Ni, Cu and Cr are low, <70, <80 and <150 ppm, respectively. Platinum and Pd concentrations were below detection limit (5 ppb) in all samples, as was Au, except for one sample from (SIKA-2017-154.2, Hongonniittu), for which the concentration was 6 ppb. Hongonniittu samples have similar geochemical signature to Palojärvi samples (Fig. 12).

Rare earth element (REE) patterns for Palojärvi intrusion samples display weak LREE enrichment over HREE (Fig. 14a, $(La/Yb)_N$ = 2.7–11.5) with Eu-anomalies varying from weakly negative to clearly positive (Eu/Eu* = 0.79–2.47). When normalized against normal mid-ocean ridge basalt (NMORB), the Palojärvi intrusions display enrichment in LILE, strong negative anomaly for Nb and a less pronounced one for Y, in addition to positive Sr anomalies (Fig. 14b).

4.4.2. Matokulma

Matokulma intrusion has median SiO_2 of 50.2 wt.% with a more restricted range (49.0–51.5 wt.%) than Palojärvi intrusions (Fig. 12a). Matokulma has limited Mg# values from 69 to 75 (Fig. 13a) and MgO concentrations from 8.3 wt.% to 15.3 wt.% (Fig. 12). Both Al_2O_3 and FeOt are lower in Matokulma than in Palojärvi intrusions, 6.23–18.97 wt.% and 7.91–13.44 wt.% respectively. MgO and Al_2O_3 correlate negatively and Al_2O_3 correlate positively with Sr. Concentrations of Cu and Ni are low and similar to Palojärvi intrusion, being <90 and <140 ppm respectively, the latter excluding an outlier of 340 ppm. Cr is distinctly higher than in Palojärvi intrusions (160–1400 ppm) and displays positive correlation with MgO. The Mg# versus CaO/Al_2O_3 plot shows (Fig. 13a) the distinctly differing fractionation trends of the intrusions with Matokulma having high values on both axes, compared to Palojärvi. Platinum, Pd, and Au were analyzed from selected pyroxene and amphibole rich samples, but all elements were below detection limit (5 ppb).

Chondrite-normalized REE patterns of the Matokulma samples display weaker LREE/HREE fractionation than Palojärvi as La/Yb_N varies from 2.9 to 3.8 (Fig. 14a), excluding one sample (SIKA-2017-6.4) with slight LREE depletion compared to MREE and La/Yb_N of 1.5. The samples show a weakly negative Eu-anomaly (0.72–0.95). On a NMORB-normalized trace element diagram (Fig. 14b), the Matokulma samples display enrichment in LILE, strong negative anomaly for Nb, and weaker ones for P, Hf, Ti and Y, in addition to positive Sr anomalies (Fig. 14b).

Matokulma dikes are more fractionated compared to the cumulate samples of the intrusion proper, with typically lower concentrations of MgO, Ni, and Cr and higher concentrations of

Table 1. Whole-rock assays for the studied intrusions. Oxides are normalized to 100% (volatile-free). Oxides and unmarked elements are analyzed with XRF from powder pellets, 1 = analyzed with ICP-OES, REE and elements with 2 with ICP-MS, n = number of analyzed samples, SD = standard deviation, <10 = below detection limit, Mg# = molar 100*MgO/(MgO+0.85*FeOt). Notice that only one sample from Hongonniittu was analyzed with ICP-MS and ICP-OES, hence the lack of ranges for REE or elements marked with 1 or 2.

Intrusion	**Matokulma**				**Matokulma dikes**				**Palojärvi**				**Hongonniittu**			
n (XRF)	19				9				36				4			
n (ICP)	6				6				9				1			
wt.%	Mean	SD	Min	Max	Mean	SD	Min	Max	Mean	SD	Min	Max	Mean	SD	Min	Max
SiO_2	50.19	0.79	48.97	51.54	51.50	1.65	49.90	55.37	45.29	3.20	39.12	52.02	44.54	1.29	43.45	46.40
TiO_2	0.52	0.11	0.37	0.72	0.98	0.16	0.83	1.37	1.39	0.58	0.44	2.75	0.93	0.43	0.48	1.33
Al_2O_3	12.04	3.70	6.23	18.03	15.95	2.01	11.89	18.97	18.40	2.93	10.44	27.47	21.72	3.05	19.04	26.11
FeOt	9.51	1.34	7.04	11.96	9.90	1.07	7.67	11.52	13.62	2.90	6.76	20.89	10.29	2.58	6.45	12.04
MnO	0.18	0.03	0.14	0.23	0.18	0.03	0.12	0.22	0.21	0.05	0.07	0.31	0.15	0.04	0.09	0.18
MgO	11.90	2.17	8.32	15.29	6.90	3.03	4.07	13.97	6.48	2.56	2.12	14.15	6.25	3.39	3.05	11.04
CaO	12.55	1.12	9.74	14.10	8.80	1.31	6.72	10.37	10.07	1.76	6.58	14.79	12.83	1.27	11.13	14.21
Na_2O	1.22	0.25	0.75	1.64	2.37	0.66	1.16	3.29	1.86	0.69	0.84	4.25	1.47	0.51	0.70	1.73
K_2O	0.64	0.25	0.36	1.43	1.83	1.08	0.65	4.15	0.71	0.41	0.20	1.73	0.47	0.09	0.37	0.56
P_2O_5	0.07	0.03	0.01	0.11	0.36	0.12	0.28	0.61	0.28	0.20	0.04	0.66	0.11	0.05	0.04	0.15
Mg#	72.0	1.7	68.6	74.7	57.3	9.0	47.9	74.4	48.6	7.6	32.5	62.9	53.7	7.9	49.5	65.5
CaO/Al_2O_3	1.15	0.42	0.65	2.26	0.56	0.10	0.41	0.72	0.55	0.08	0.42	0.78	0.59	0.04	0.54	0.62
ppm																
Ba	137	92	30	380	540	317	170	1290	248	162	60	750	103	39	50	140
Co[1]	56.1	5.1	50.0	65.0	35.6	8.2	28.9	50.8	52.1	24.0	16.2	90.0	66.4	-	-	-
Cr	856	406	160	1400	314	347	30	1010	43	27	20	150	98	38	60	150
Cu	55	17	20	90	45	23	20	70	46	14	20	80	45	17	20	60
Hf[2]	0.7	0.1	0.7	0.8	2.4	1.3	1.6	5.0	2.2	1.4	0.7	4.9	2.0	-	-	-
Ni	99	65	40	340	114	127	30	400	37	14	20	70	40	8	30	50
Rb[1]	18.7	6.3	14.5	31.0	46.6	24.2	23.1	77.8	14.2	8.8	3.6	29.4	13.5	-	-	-
S	922	531	200	2500	371	287	100	900	647	410	100	1600	500	356	200	900
Sc[1]	58.2	5.5	51.8	67.6	33.2	3.3	27.8	36.0	22.9	16.6	3.5	58.4	15.8	-	-	-
Sr	359	150	140	630	552	142	310	730	599	168	210	1020	680	104	590	830
V	258	47	170	360	211	28	150	240	347	145	90	780	353	162	180	500
Nb[2]	<3				5.4	3.1	3.1	11.3	6.7	4.9	3.3	14.0	<3			
Ta[2]	<1				<1				1.28	-	-	-	<1			
Th[2]	<2				2.3	0.1	2.1	2.5	5.1	5.0	2.0	10.8	<2			
U[2]	0.4	0.1	0.3	0.5	0.8	0.4	0.5	1.7	0.6	0.6	0.3	2.1	0.2	-	-	-
Y[1]	11.2	1.3	9.2	12.8	16.4	4.1	12.1	23.3	12.6	12.1	3.8	43.3	2.7	-	-	-
Zn	82	15	60	110	112	16	90	130	128	30	60	180	83	17	60	100
Zr	48	10	30	60	98	33	70	170	66	21	20	130	60	8	50	70
La	5.5	1.9	2.1	7.9	14.4	4.2	9.8	22.1	9.9	6.4	3.3	22.5	3.3	-	-	-
Ce	13.9	4.1	6.4	18.7	33.3	10.8	21.8	53.7	23.5	17.6	8.5	64.4	8.9	-	-	-
Pr	2.0	0.5	1.2	2.6	4.5	1.6	2.9	7.6	3.2	2.6	1.2	9.5	0.8	-	-	-
Nd	9.9	2.0	6.4	12.1	20.4	7.2	13.0	34.2	13.9	11.6	5.3	43.1	3.5	-	-	-
Sm	2.6	0.4	2.0	3.0	4.5	1.5	3.1	7.4	3.1	2.7	1.2	10.0	0.8	-	-	-
Eu	0.7	0.1	0.7	0.8	1.5	0.4	1.1	2.2	1.2	0.7	0.5	2.7	0.4	-	-	-
Gd	2.7	0.4	2.1	3.1	4.3	1.3	3.1	6.7	3.1	2.7	1.2	9.9	0.8	-	-	-
Tb	0.4	0.1	0.4	0.5	0.7	0.2	0.5	1.0	0.5	0.4	0.2	1.6	0.1	-	-	-
Dy	2.7	0.4	2.2	3.1	3.9	1.0	3.0	5.6	2.9	2.6	1.1	9.5	0.8	-	-	-
Ho	0.5	0.1	0.4	0.6	0.8	0.2	0.6	1.1	0.6	0.5	0.2	1.9	0.2	-	-	-
Er	1.5	0.2	1.2	1.7	2.1	0.5	1.6	3.1	1.7	1.5	0.6	5.6	0.5	-	-	-
Tm	0.2	0.0	0.2	0.2	0.3	0.1	0.2	0.4	0.2	0.2	0.1	0.8	<0.1	-	-	-
Yb	1.2	0.2	1.0	1.4	1.9	0.4	1.4	2.6	1.5	1.3	0.6	4.8	0.4	-	-	-
Lu	0.2	0.0	0.2	0.2	0.3	0.1	0.2	0.4	0.3	0.2	0.1	0.7	<0.1	-	-	-

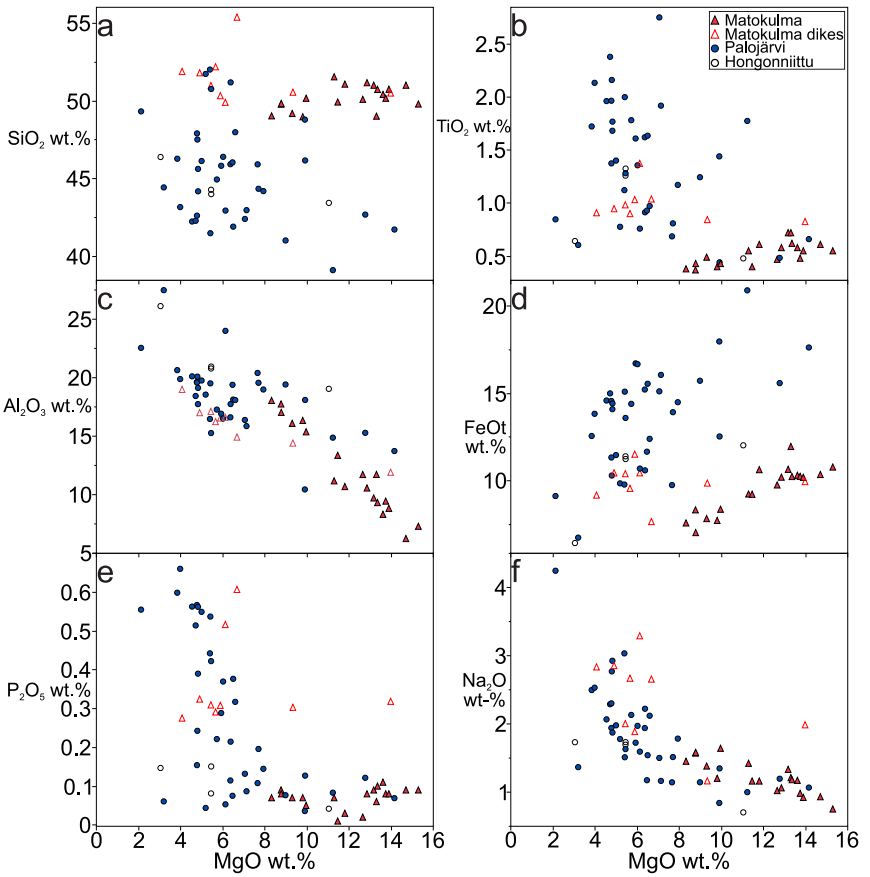

Figure 12. Binary diagrams of whole-rock MgO versus a) SiO_2, b) TiO_2, c) Al_2O_3, d) total iron as FeO (FeOt), e) P_2O_5, f) Na_2O. Matokulma samples all have similar SiO_2, at ~50 wt.% and relatively high MgO. Palojärvi intrusion is more fractionated, with higher concentrations of TiO_2, FeOt, and P_2O_5 than Matokulma but with typically lower SiO_2. With decreasing MgO, the concentrations of Al_2O_3, Na_2O, P_2O_5 increase. All oxides are presented as volatile-free (normalized).

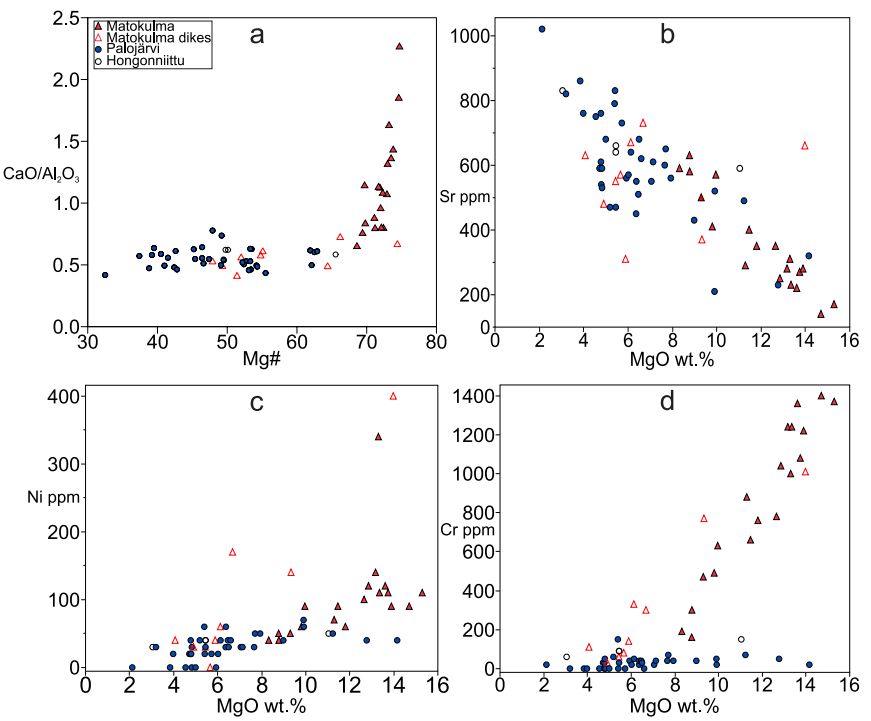

Figure 13. Binary diagrams of whole-rock chemistry Mg# (a) and MgO (b,c,d) versus a) CaO/Al_2O_3, b) Sr, c) Ni, d) Cr. Matokulma has the highest Mg#, CaO/Al_2O_3, Cr, and Ni of the studied intrusions. With increasing fractionation (decreasing MgO and Mg#), concentrations of Cr and Ni decrease and the concentration of Sr increases. Mg# is molar MgO/(MgO+0.85FeOt).

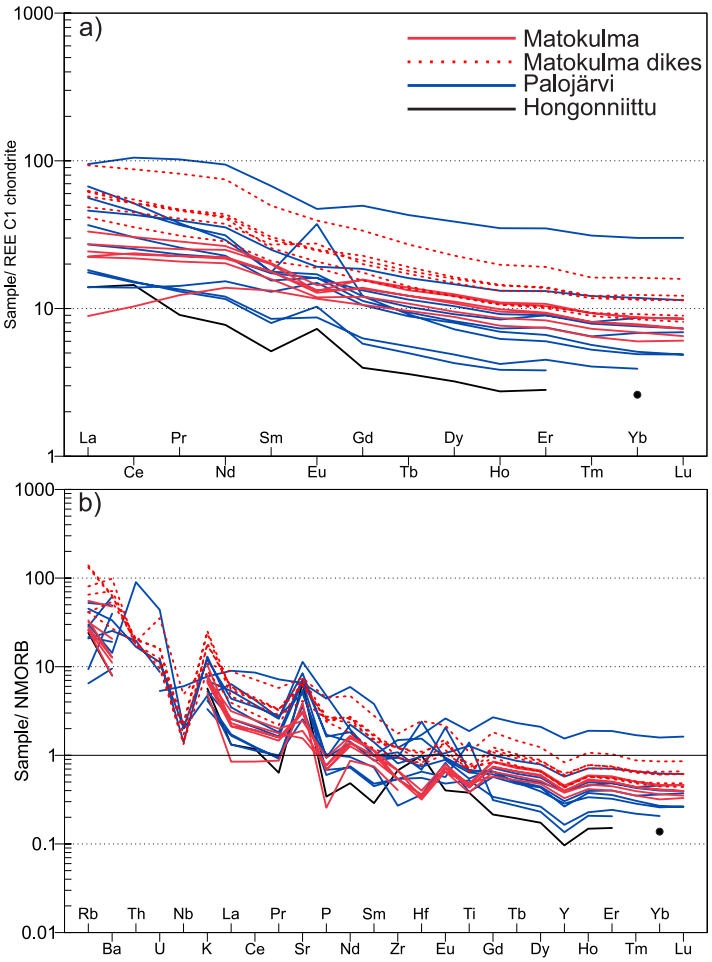

Figure 14. a) Samples from all intrusions show similar trends with enrichment in LREE. Some samples have negative (Matokulma) and some samples from Palojärvi positive Eu anomalies. Ultramafic sample from Matokulma (SIKA-2017-6.4) is depleted in LREE. a) Normalized against C1 chondrite (McDonough and Sun, 1995). b) NMORB (Sun and McDonough, 1989) normalized trace element diagram for the samples examined in this study. Note that in 11 out of 21 samples Nb was below the detection limit (3 ppm). Similarly, 13/21 samples had Th below detection limit (2 ppm).

TiO_2, Al_2O_3, P_2O_5, and Sr. Dikes from Matokulma have moderately fractionated REE patterns (La/Yb_N = 4.2–6.9) and lack significant Eu-anomalies with Eu/Eu* from 0.92 to 1.14. On NMORB-normalised spider diagram, the dike samples have the same Nb, Sr, Ti, and Y anomalies as the samples from the intrusion proper, but they lack the Hf and P anomalies (Fig. 14b).

4.5. Isotope geochemistry

4.5.1. Age determinations

Sample A2463 Palojärvi represents a leucocratic gabbro dike crosscutting the central part of the Palojärvi intrusion and is interpreted to represent late melt fractions of the intrusion, based on the fractionated geochemistry (lowest MgO, Mg#, Cr and highest Sr (Fig. 13) and, La/Yb_N, Fig. 14a). Zircon crystals are mostly subhedral to euhedral, 100–150 µm long and some of them display oscillatory zoning. Altogether 20 spots from as many individual crystals were analysed.

All of the analyses (Electronic Appendix A) are concordant or nearly concordant and cluster relatively tightly (Fig. 15a), but do not allow calculation of a concordia age. Correlation between zircon composition and age does not exist. Therefore, we regard the weighted average of $^{207}Pb/^{206}Pb$-ages of all spots, 1882 ± 5 Ma, as the best estimate for the crystallization age of this sample.

Sample A2464 Haukkavuori represents the leucocratic biotite-amphibole granite bordering

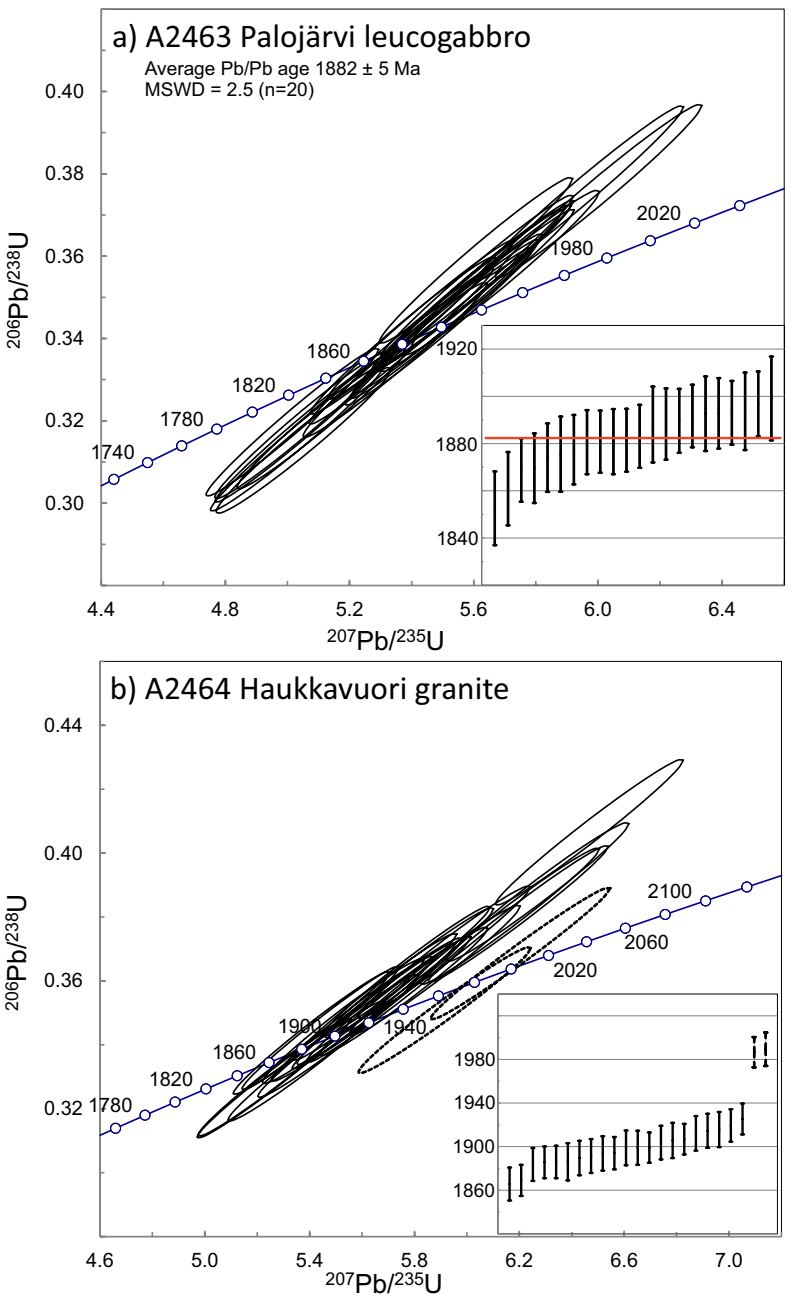

Figure 15. a) Concordia diagram for sample A2463 Palojärvi, as inset the $^{207}Pb/^{206}Pb$ –ages, whose weighted average of 1882 ± 5 Ma is interpreted as the crystallization age. b) Concordia diagram for sample A2464 Haukkavuori, dashed ellipses mark analyses interpreted as clearly inherited. As inset the 207Pb/206Pb –ages of the zircons, see text for further discussion. All data plotted at 2σ level.

the Palojärvi west intrusion to the south and crosscutting it. The zircon grains are typically euhedral and resorbed and display zoned growth textures. Metamict domains are relatively common. Altogether 23 spots representing 21 separate crystals were analysed.

All analyses are either concordant or reversely concordant (Fig. 15b; Electronic Appendix A). Two of the spots yield distinctly older $^{207}Pb/^{206}Pb$ ages, 1989 ± 8 Ma and 1987 ± 7 Ma. These crystals are interpreted as inherited. $^{207}Pb/^{206}Pb$ ages of the remaining 21 spots scatter from 1925 to 1866 Ma and average at 1897 ± 7 Ma with a high MSWD value of 4.3. Two of the youngest spots are

Table 2. Whole-rock Nd isotope composition of the Palojärvi leucogabbro (A2463) and Haukkavuori granite (A2464)

Sample name	A2463	A2464
Sm (ppm)	1.56	2.54
Nd (ppm)	8.78	17.87
$^{147}Sm/^{144}Nd$	0.1076	0.0858
$^{143}Nd/^{144}Nd_a$	0.511666 ± 0.000009	0.511339 ± 0.000007
$\varepsilon_{Nd\ i}$ (at 1880 Ma)$_b$	2.6	1.5
T_{DM} (Ma)$_c$	1923	1980

Note: Isotopic analyses at the Geological Survey of Finland (GTK).

a $^{143}Nd/^{144}Nd$ normalized to $^{146}Nd/^{144}Nd = 0.7219$; reported error is 2σ.

b Initial Nd isotope composition expressed as the ε_{Nd} value, calculated using $^{143}Nd/^{144}Nd = 0.512638$ and $^{147}Sm/^{144}Nd = 0.1967$. External error is ± 0.4 ε units.

c Depleted mantle model age (DePaolo 1981).

from the same crystal. It is highly likely that also the screened (21/23) spots include xenocrystic zircon and hence the 1897 ± 7 Ma age cannot be considered as the crystallization age of the granite. Field evidence (varying cross-cutting relationships, mingling structures) rather suggests that the granite south of Palojärvi intrusion is either younger or consanquineous with the gabbro. Regardless of the granite's exact age, an interesting feature is the abundance of zircons aged 1.93–1.91 Ga, i.e., older Svecofennian magmatism (Huhma et al. 2021).

4.5.2. Sm-Nd

The whole-rock Nd isotope data measured for the two samples from the Palojärvi intrusion area are shown in Table 2. The leucocratic gabbro dike (sample A2463) that cuts the north-central part of the Palojärvi intrusion has low Sm and Nd content (1.56 and 8.78 ppm, respectively), a low $^{147}Sm/^{144}Nd$ ratio of 0.1076 and is relatively radiogenic with an ε_{Nd}(1880 Ma) value of +2.6 ± 0.4. The depleted mantle model age, 1923 Ma, is slightly higher than the crystallization age of the dike. The biotite-hornblende granite (sample A2462) from the southern fringe of the Palojärvi intrusion has 2.5 ppm Sm, 17.87 ppm Nd and is strongly enriched in LREE with a $^{147}Sm/^{144}Nd$ of 0.0858. The ε_{Nd}(1880 Ma) value of the granite is +1.5 ± 0.4 and the depleted mantle model age 1980 Ma.

4.6. Gravity data

Modelling of the gravity data was done using laboratory measured average densities of hand samples, which are for Matokulma 2 984 kg/m^3, Palojärvi 3 020 kg/m^3 and Hongonniittu 2 987 kg/m^3, respectively. A density of 2 670 kg/m^3 was used for the country rock. Based on modelling of gravity data, Palojärvi is a nearly vertical, rectangular body with depth extent of ca. 850 m (Fig. 3). Hongonniittu dips northwards in angle of ca. 47° and continues to depth of ca. 700 m. Matokulma intrusion is more irregularly shaped (Fig. 6). Data from the eastern line indicates that the intrusion dips in a shallow angle and continues below surface ca. 200 m north of the contact observed in the field. Along Matokulma's western profile the intrusion dips more steeply towards north and the data implies presence of less dense material in central part of the intrusion. Based on modelling the depth extent of the Matokulma intrusion along both lines is just 200–250 m. Models and their calculation parameters can be found in Karvinen (2019, unpublished Master's thesis).

5. Discussion

5.1. Constrains on the parental magma composition

5.1.1. Parental magma calculations

As chilled margins were not found, the mineral chemistry of the primary, early crystallizing mafic minerals (primarily orthopyroxene) was used to estimate the parental magma composition. This method is based on assumption that the minerals were in equilibrium with the magma during crystallization. The magnesium endmembers of olivine and orthopyroxene can be used to determine the FeO/MgO ratio of the magma from which the minerals crystallized from (e.g., Roeder & Emslie 1970). Partition coefficient (K_D) for partitioning of iron and magnesium between melt and olivine is experimentally determined to be 0.30±0.03 and independent of temperature at a pressure of 1 atm (Roeder & Emslie 1970; Roeder 1974).

$$K_D = \frac{\left(X_{FeO}^{Ol}\right)}{\left(X_{FeO}^{Liq}\right)} \frac{\left(X_{MgO}^{Liq}\right)}{\left(X_{MgO}^{Ol}\right)} \qquad (eq.\,1)$$

The results of Roeder and Emslie (1970) have been widely applied, but also criticised as the partition coefficient is affected, in addition to the composition of the magma, also by the pressure and temperature of the system (e.g., Herzberg & O'Hara 2002; Toplis 2005). However, the K_D value of ~0.30 is considered valid for basaltic systems at pressures of < 2-3 GPa (Toplis 2005; Putirka 2008).

Makkonen (1996) applied the exchange coefficients of Roeder & Emslie (1970) to estimate the MgO concentrations of Kotalahti type parental magmas based on the forsterite (Fo) or enstatite (En) endmember components of olivine or orthopyroxene, respectively. The equations conform to the MgO/FeO ratio of the Svecofennian tholeiites-picrites, which are considered to be comagmatic with the Svecofennian mafic-ultramafic intrusions (e.g., Makkonen & Huhma 2007; Barnes et al. 2009) and can be used only for magma types of similar MgO/FeO ratios (Makkonen et al. 2017).

The equation for Fo (KD = 0.33) is

$$\log MgO_{liq} = \frac{\log Fo - \log(252.7833 - 0.7825Fo)}{0.4602} + 1.795 \qquad (eq.\,2)$$

For En (K_D = 0.23);

$$\log MgO_{liq} = \frac{\log En - \log(36268.9182 - 188.1602En)}{0.4602} + 6.1409 \qquad (eq.\,3)$$

In the absence of primary olivine or orthopyroxene, the parental magma composition can be approximated from the whole-rock chemistry by calculating a hypothetical (Fo) or (En) composition, based on the molar ratio of MgO to FeO_t:

$$b = \frac{MgO\ m\text{-}\%}{FeO_t\ m\text{-}\%} \qquad (eq.\,4)$$

$$Fo,En = \frac{b}{1+b} \qquad (eq.\,5)$$

Plotting all whole-rock samples on Pearce's (1968) molar ratio diagrams where MgO and FeO are normalized with Al_2O_3 or TiO_2 (or some other incompatible elements) can be used to determine the MgO/FeO ratio of the parental magma, based on the slope of the regression line. The slope gives the molar ratio of MgO to FeO. If all iron is assumed to be Fe^{2+}, the slope gives the MgO/FeO ratio directly. This ratio is then used to calculate Fo or En content of the mineral that controls the fractionation. The Fo, En content is then input into equation 2 or 3, respectively, which gives the MgO concentration (wt.%) of the melt. Mg# of the magma can be calculated with the MgO/FeO ratio together with the partition coefficient K_D, which can then be used to calculate the FeO_t concentration. As the studied intrusions are composed of evolved rocks related to Paleoproterozoic arc-magmatism, the iron is not solely bivalent (e.g., Kelley & Cottrell, 2009), thus we cannot assume Fe^{2+}/Fe_{tot} =1. Instead, a Fe^{2+}/Fe_{total} ratio of 0.85 was utilized.

Using these formulas, we calculated an approximation of the parental magma composition for both Matokulma and Palojärvi intrusions (Electronic Appendix B). As these intrusions consist mostly of evolved, plagioclase-bearing cumulates with clinopyroxene ± orthopyroxene and intercumulus amphibole, rather than olivine or pyroxene cumulates, the calculations below give estimates of the MgO concentration of the parental magmas to be used later in the discussion regarding the ore potential of the intrusions, together with relevant trace element concentrations.

5.1.2. Palojärvi

TiO_2 was used for normalisation and parental magma calculations for the Palojärvi intrusion, yielding a good fit (R^2 = 0.9609, Fig. 16). The Fo, En content based on the regression line is 66.

If olivine was the controlling cumulus mineral, the MgO concentration of the magma would have been5.53 wt.% and FeOt 13.1 wt.%. The Mg# of the magma would have been 39. If orthopyroxene had been the sole cumulus mineral, the MgO and FeO concentrations of the magma would have been 3.82 ± 0.15 wt.% and 12.98 ± 0.15 wt.%, respectively. Mg# would have been 31.

Composition of cumulus olivine in sample SIKA-2017-80.1 ranges from Fo_{42} to Fo_{46}, noticeably less magnesian than the calculated Fo based on the Pearce diagram (Fo_{66}, Fig. 16) and the calculated equilibrium MgO concentration in the parental magma is on median 1.99 wt.% (1.75–2.27 wt.%). Interstitial orthopyroxene in same sample has a compositional range of $En_{52–60}$ with the calculated magma MgO concentrations ranging from 1.86 wt.% to 2.73 wt.%, with a median value of 2.31 wt.%.

Orthopyroxene from other samples have lower En compositions and consequently lower calculated MgO_{liq} concentrations, which range from 0.94 wt.% up to 2.23 wt.%.

Based on the results above, the Palojärvi parental magma contained 2–4 wt.% MgO.

5.1.3. Matokulma

Al_2O_3 was used for normalizing MgO and FeOt in Matokulma samples in the Pearce diagram (Fig. 17). The Fo, En content based on the regression line is 75. The MgO content of the magma (MgO_{liq}), calculated on the basis of the Fo content, is 7.96 ± 0.18 wt.%. Mg# of the magma was 50 and the FeO_t concentration based on the Mg# is 12.05 wt.%.

If orthopyroxene would have been the mineral first to crystallize, the MgO_{liq} is calculated to be 5.98 ± 0.13 wt.% with a Mg# of 41 and a FeO_t concentration of 12.99 wt.%. As the studied rock types in Matokulma contain no olivine, at least at the present erosional level, orthopyroxene is used for the calculation basis of the parental magma.

The highest obtained MgO_{liq} value, 5.58 wt.% was calculated from a single analyzed poikilitic orthopyroxene grain from sample SIKA-2017-173, with En_{74}. The euhedral cumulus orthopyroxene in sample SIKA-2017-115.2 yielded median MgO_{liq} value of 4.92 wt.% MgO with a range of 3.74 to 5.24 wt.% MgO. The enstatite content and the

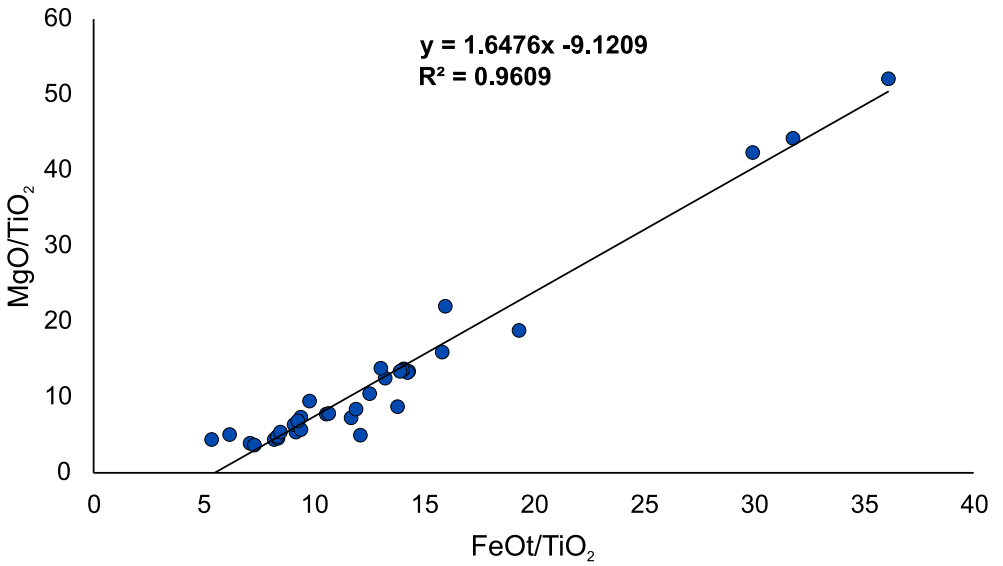

Figure 16. Mafic-ultramafic Palojärvi samples plotted on a Pearce (1968) molar ratio diagram with TiO_2 normalised FeOt and MgO plotted against each other. The samples fit the regression line well (R^2=0.9609). The three samples with highest MgO and FeO are amphibole rich.

calculated MgO_{liq} are similar to the one calculated from whole-rock compositions within 0.3 wt.%.

The dike rocks display scatter in Pearce diagrams, likely due to alteration, and cannot be used in regression calculations. However, using equations 4 and 5 to calculate hypothetical mineral compositions and then placing these into equations 2 and 3 yielded median MgO_{liq} concentrations of 3.38 wt.% and 2.13 wt.%, for forsterite and enstatite, respectively. The highest value obtained was from sample SIKA-2017-119.1, which yielded 7.73 wt.% and 5.77 wt.% MgO_{liq}, for hypothetical forsterite and enstatite, respectively.

Based on these calculations, the Matokulma parental magma contained 5–6 wt.% MgO.

5.2. Whole-rock and mineral chemical constraints on magmatic evolution of Matokulma and Palojärvi

The results and calculations presented in the previous chapters show that the studied intrusions are cumulate rocks fractionated from evolved magmas. Primary magmas in equilibrium with mantle peridotite have Mg# of ~70 (e.g., Roeder & Emslie 1970; Green et al. 1974; Falloon & Green 1987; Gaetani et al. 1998) compared that to maximum calculated values of 50 and 39 for Matokulma and Palojärvi, respectively.

5.2.1. Fractionation trends

The differing magmatic evolutionary paths of the intrusions are well exhibited in whole-rock CaO/Al_2O_3 versus Mg# and MgO versus Al_2O_3, P_2O_5, Cr, and Sr diagrams (Fig. 12 and 13). Matokulma gabbros have relatively high and constant Mg# and CaO/Al_2O_3 (Fig. 13a), the latter decreasing with Cr and V.

Based on petrography, clinopyroxene is the earliest cumulate phase in Matokulma. The clinopyroxene have a similar median Mg# of ~79 in all analyzed samples. These trends are consistent with progressive fractionation and modal decrease of clinopyroxene ± chromite and increase of plagioclase, which indicates that clinopyroxene controlled the evolution of the parental magma (e.g., Bender et al. 1978). In Palojärvi, all rock types are depleted in Cr (Fig. 13d) and have constant CaO/Al_2O_3 ratios (Fig. 13a). Magnesium numbers are typically below 50, but up to 65 in amphibole-rich samples (Fig. 13a).

Natural and experimental orthopyroxene

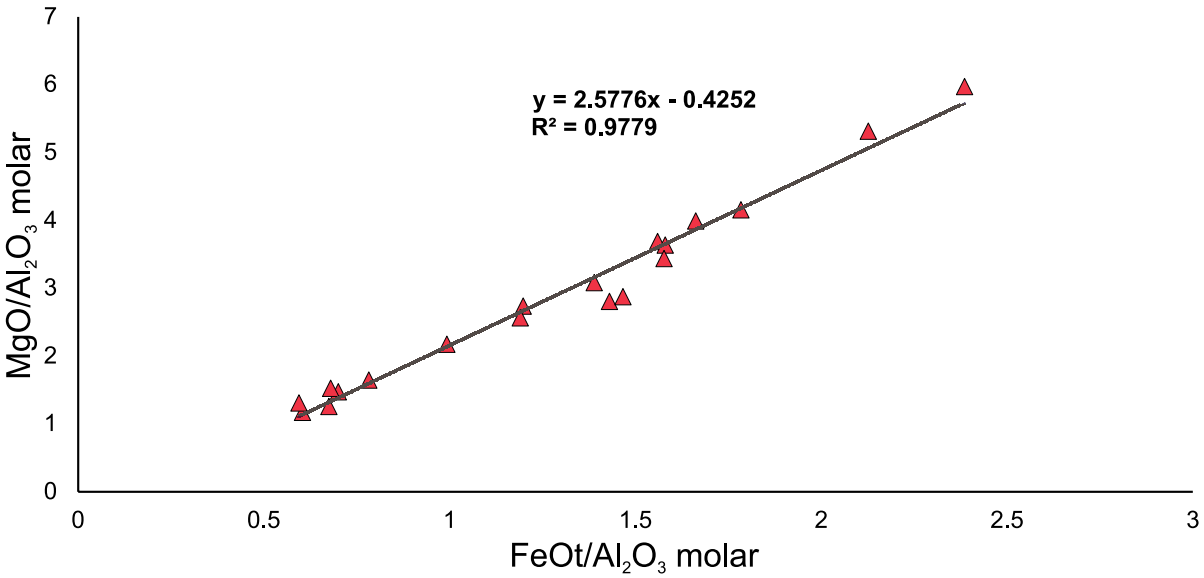

Figure 17. Matokulma samples plotted on a Pearce (1968) $FeOt/Al_2O_3$ vs. MgO/Al_2O_3 molar ratio diagram.The samples fit the regression line well (R^2=0.9779).

and clinopyroxene crystallized from hydrous arc magmas under high pressure conditions are enriched in Al, if there are no liquidus Al-phases (Elthon et al. 1982, DeBari & Coleman 1989, Müntener et al. 2001). Increasing degree of crystallization also increase the concentrations of Al_2O_3 and FeO in pyroxene (Bender et al. 1978). These Al and Cr enriched clinopyroxene crystals may have crystallised earlier in the evolution of the parental magma, before the onset of plagioclase crystallization and/or at higher pressures (e.g., Villiger et al. 2007).

5.2.2. Whole-rock trace element systematics

The intrusions have similar REE patterns with weak LREE/HREE fractionation, and a flat HREE trend. Differences due to fractionation of plagioclase can be observed as positive Eu-anomalies in Palojärvi intrusions and negative in Matokulma, caused by the accumulation and removal of plagioclase from the parental magma, respectively. In Matokulma, the dike rocks are more enriched in REE than the gabbros, lack Eu-anomaly but otherwise exhibit similar REE fractionation patterns, indicating crystallization from a common parental magma (Fig. 14a). The most primitive sample from Matokulma is from an ultramafic layer (SIKA-2017-6.4) depleted in LREE and with the lowest REE concentration of all the samples.

The 'spiky' trend seen in MORB-normalized trace element diagrams is often referred to as 'arc signature' (Fig. 18; e.g., Tatsumi & Kogiso 2003; Zellmer et al. 2015) caused by subduction-related fluid metasomatism. A residual titanate phase (e.g., rutile, titanite) has high partition coefficients for high field strength elements (HFSE), thus it depletes these elements from fluids during dehydration of slab subduction (McCulloch & Gamble 1991; Green 1994; Foley et al. 2000). The presence of refractory amphibole in the dehydrating slab might also cause a similar signature (Woodhead et al. 1993). Early fractionation of Fe-Ti-oxides can also deplete HFSE from the magma (Klemme et al. 2006).

The Palojärvi samples display more scatter in trace element diagrams, especially in middle

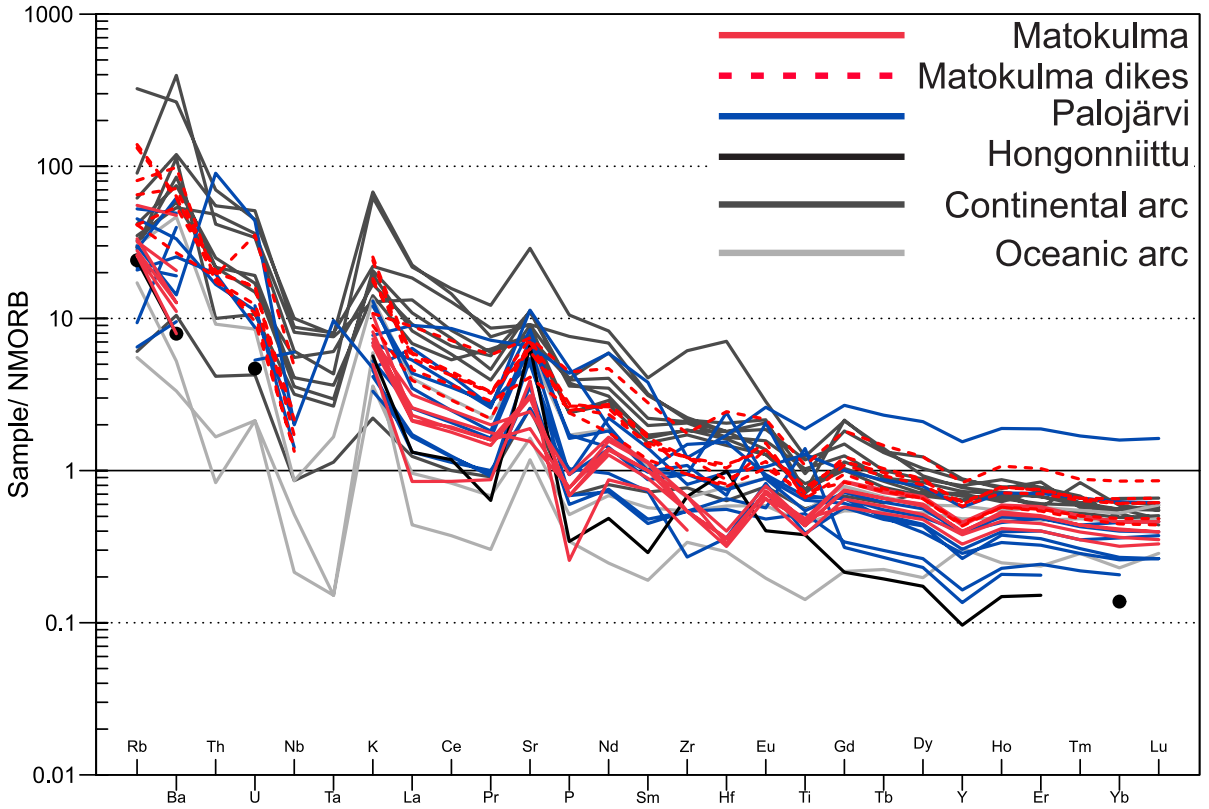

Figure 18. NMORB (Sun and McDonough, 1989) normalized whole-rock trace element diagram with the studied samples and reference arc type basalts and andesites (dark gray, continental arc; light gray, oceanic arc; reference compositions from; Scmidt and Jagouz, 2017). Black dots indicate Hongonniittu outside of the continuous lines.

REE and Nb, Zr, and Hf. Enrichment in large ion lithophile elements (LILE) is similar to that of Matokulma. Some samples exhibit negative Ti-anomalies and some positive anomalies. This is likely caused by incorporation of Ti into silicate phases, especially amphibole, and the abundant Fe-Ti-oxides.

The more evolved composition of Palojärvi is evident from the strong depletion of mantle-compatible elements (i.e., Ni and Cr; Fig. 13c, d). Even in the olivine-hornblende norite (SIKA-2017-80.1, Fig. 8), the whole-rock Ni concentration is only 50 ppm.

Palojärvi sample SIKA-2017-54.1 differs from other samples with noticeably higher REE and other trace elements. This sample has also the highest TiO_2 and Y concentrations (2.4 wt.%, 43 ppm, respectively; Fig. 12b). This is most likely caused by large amount of amphibole + biotite (Claeson & Meurer 2004), and fine-grained magnetite dissemination.

5.3. Comparison to Vammala and Kotalahti type intrusions and evaluation of ore potential

The Vammala and Kotalahti type intrusions are olivine-rich cumulates with Ni-Cu potential, crystallized from relatively primitive magmas with 10–12 wt.% MgO (Makkonen et al. 2017). These magmas achieved sulphide saturation through assimilation of carbonate and sulphide bearing black schists (Peltonen 2005) and are markedly different from the gabbroic intrusions described in this study that crystallized from evolved magmas.

The differences to the Vammala and Kotalahti type intrusions are clearly presented also on ternary CaO-MgO-Al_2O_3 (CMA) and Al_2O_3-FeO_t-MgO (AFM) diagrams (Fig. 19). Most samples plot on the tholeiitic trend (Fig. 19a), except for the majority of Matokulma dike rocks. The ore potential intrusions plot close to the MgO vertices due to their, olivine-rich cumulate compositions. Note that the ore potential Kotalahti-type intrusions are more Al-rich than the barren ones, probably because of assimilation of felsic crustal rocks (Makkonen et al., 2008). The intrusions studied here, as well as the nearby Kaipola layered intrusion (Peltonen & Elo 1999; Nironen et al. 2000; Peltonen 2005) are gabbroic in bulk composition, clearly less magnesian and contain more alkalis and aluminium than the ore potential intrusions (Fig. 19a, b). The overall gabbroic compositions indicate fractionation from an evolved magma, rather than a primitive one.

One conspicuous similarity is the presence of magmatic interstitial amphibole, present in Vammala and Kotalahti type intrusions, Kaipola layered intrusion (Makkonen 1996, Lamberg 2005, Peltonen 2005) and in the intrusions studied here. Peltonen (2005) interpreted the amphibole as a late-magmatic phase, formed in a peritectic reaction between cumulus pyroxenes and the residual hydrous melt. In the studied samples, cumulus clinopyroxene and plagioclase grains are often at least partially resorbed and display a reaction rim with the poikilitic amphibole, which indicates that the cumulus phases reacted with the residual melt to form amphibole (e.g., Powell 1978, Conrad & Kay 1984). For example, in sample SIKA-2017-173.1, a cumulus diopside with 1300 ppm Cr has a rim of magnesio-hastingsite amphibole with 3900 ppm Cr. This is enclosed in magnesio-hornblende with 1490 ppm Cr, which is within a poikilitic orthopyroxene with 150 ppm Cr. We conclude that the poikilitic amphibole, present in most samples, is a late-magmatic peritectic phase also in the Palojärvi and Matokulma intrusions.

The 1882 ± 5 Ma minimum age obtained for the Palojärvi intrusion from the leucogabbro dike is contemporaneous with the Ni-Cu mineralized Vammala and Kotalahti type intrusions and also the unmineralized Kaipola layered intrusion (~1880 Ma, Peltonen 2005).

The ore potential of intrusions can be evaluated using whole-rock and mineral geochemistry by examining the magnesium content (Mg#) and Ni, Cr content of early crystallizing olivine, orthopyroxene and spinel (e.g., Häkli 1971; Makkonen 1996, Lamberg 2005). The MgO versus Ni diagram can be used to evaluate the Ni mineralization potential of an intrusion. The most potential intrusions have samples with both undepleted and depleted character, indicating depletion of nickel near the current erosion level (Makkonen et al. 2008, 2017). The samples of the studied intrusions show distinct nickel depletion (Fig. 20). For the samples of higher MgO (around > 8 wt.%) the low nickel content, compared to the model curve, is also because the dominating mafic mineral is amphibole or pyroxene, not olivine like in most samples used to draw the model curve.

In Matokulma, the Mg# range of orthopyroxenes is 67–76 and the mean Ni concentration (60 ppm) is identical to that of orthopyroxenes in Svecofennian quartz diorites (Häkli 1971). The low whole-rock and mineral Mg# and Ni indicate that the concentrations of MgO and Ni in the parental magma were low.

Owing to the evolved composition of Matokulma and Palojärvi intrusions, they have low potential for Ni-Cu-PGE mineralizations. Very strong depletion of Ni and PGE indicate that sulphide saturation has probably taken place during the evolution of the parental magmas, prior to final emplacement. In addition, olivine fractionation prior to the final emplacement level may have contributed to the depletion o f Ni.

Theoretically, Palojärvi could host a Ti-V mineralization as the few analyzed magnetites have elevated concentrations of V (1.2–1.4 wt.% V_2O_3). As magmatic layering is seen on the current erosional level, it is possible there are Fe-Ti-V oxide-rich layers deeper in the stratigraphy of the intrusion, as the gravity survey and modelling

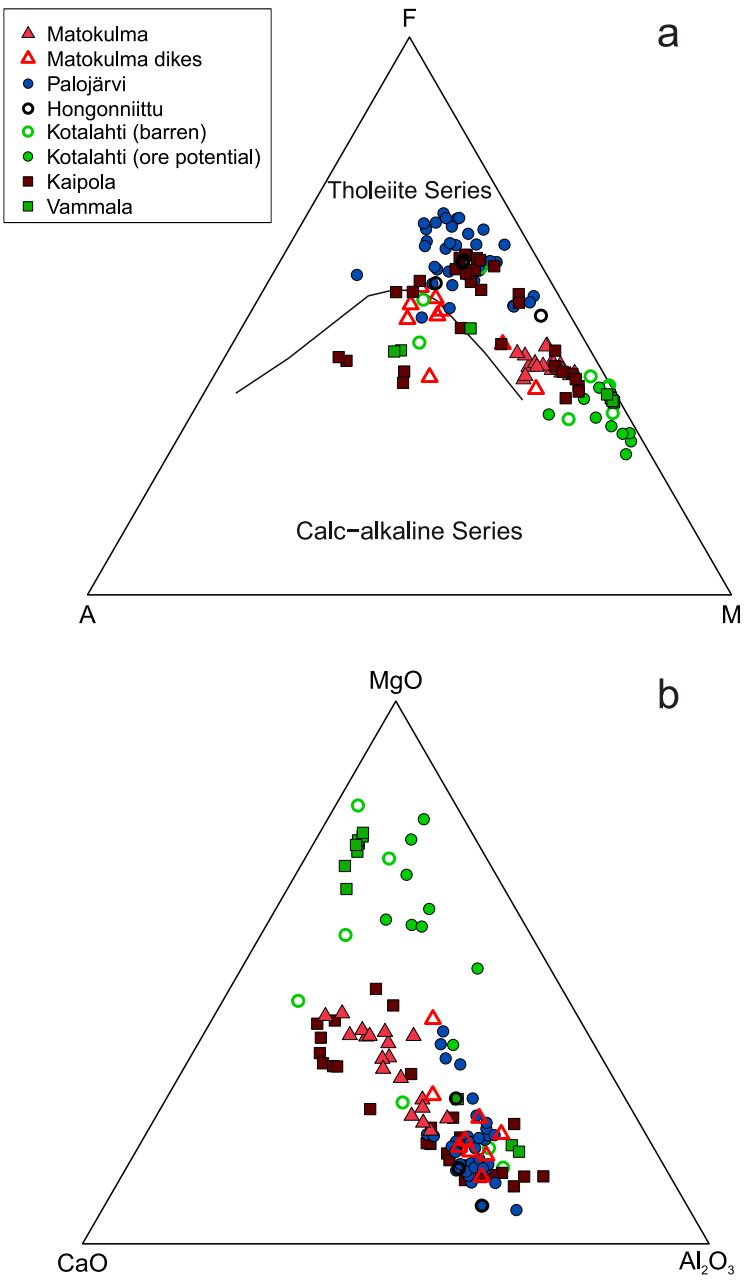

Figure 19. a) Al_2O_3-FeOt-MgO (AFM) diagram (Irvine & Baragar 1971) diagram and b) ternary CaO-MgO-Al_2O_3 (CMA) diagram of the studied intrusions, together with reference data from Vammala and Kotalahti belts and Kaipola layered intrusion. a) shows that the studied intrusions follow the same tholeiitic fractionation trend as Kotalahti and Vammala intrusions, but even the most mafic compositions are significantly more evolved. b) The studied intrusions mainly follow the "barren trend" of the Kotalahti type intrusions, instead of the ore potential, CaO poorer and orthopyroxene-plagioclase dominated fractionation trend caused by increased silica concentration during country rock assimilation. Kaipola and Vammala data from P. Peltonen (unpublished data), Kotalahti data from Makkonen et al. (2008).

results suggest that the intrusion has a depth extent of approximately 800 m. Gabbros with such mineralizations are known within the CFGC (e.g., Kärkkäinen & Bornhorst 2003; Peltonen 2005).

The enrichment of V into magnetites happens at a narrow oxygen fugacity (fO_2) range, between NNO and NNO-1.5 (Nickel-Nickel oxide buffer; Reynolds 1985; Toplis & Corgne 2002). The concentration of V in the melt decreases rapidly with the crystallization of V-rich magnetite (Toplis & Corgne 2002, Cawthorn et al. 2005). Thus, the most vanadiferous magnetite are most likely found deeper in stratigraphic height of a layered intrusion where the earliest magnetites accumulated, assuming the suitable fO_2 was attained in the evolution of the parental magma. This is observed in

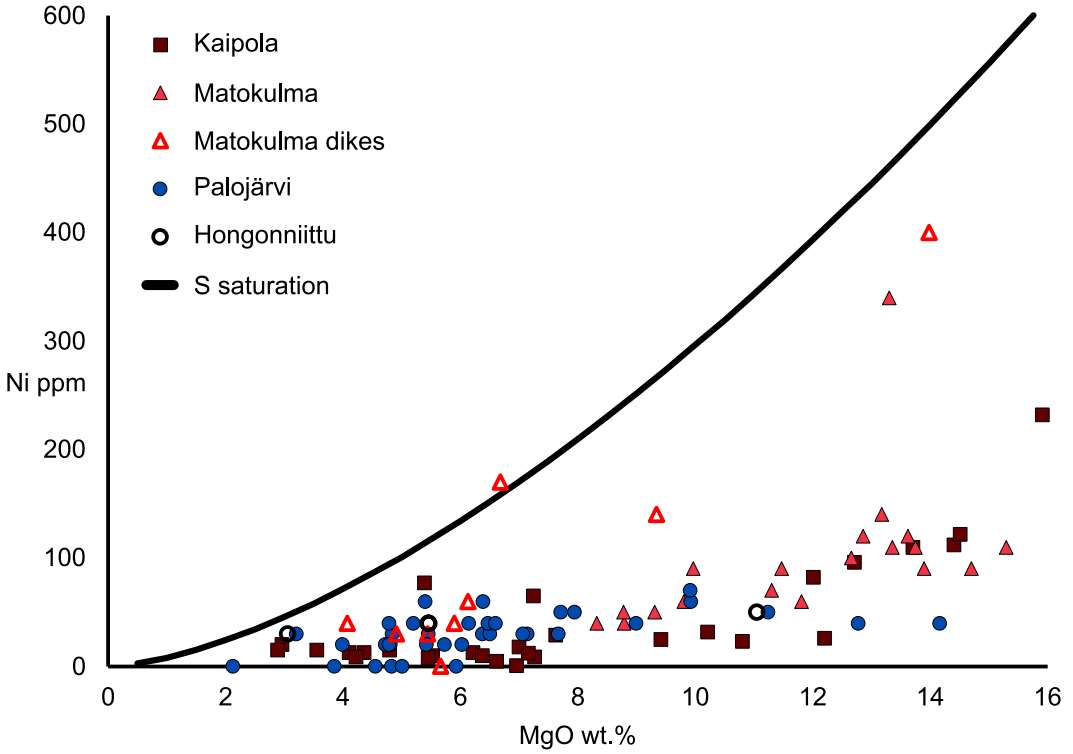

Figure 20. MgO (volatile-free) versus Ni diagram, featuring the studied intrusions and reference samples from the nearby Kaipola layered intrusion. The equation for the curve representing Ni depletion is $8.36*MgO^{1.55}$ (Makkonen et al. 2017). Excluding one dike sample from Matokulma, all the samples plot below the curve, indicating depletion in Ni. Kaipola data from P. Peltonen (unpublished).

monomineralic magnetite layers, most notably the Main Magnetitite Layer of the Bushveld intrusion (e.g., Klemm et al. 1985; Cawthorn et al. 2005) and in magnetite-rich layers in other layered intrusions like Skaergaard layered intrusion in Greenland (Vincent & Phillips 1954) and Fedorivka layered intrusion in Ukraine (Duchesne et al. 2006).

5.4. Neodymium isotope constraints on lithospheric architecture

The studied intrusions are located in the south-central part of the Central Finland Granitoid Complex (CFGC; Fig. 1). Regarding Svecofennian mafic-ultramafic plutonites, the CFGC region is characterized by Ti-Fe-P gabbros that have the traits of anorogenic gabbros and were probably emplaced in a post-kinematic tectonic regime at ≤ 1880 Ma (Peltonen 2005). About 100 km northeast of the studied intrusions, the synorogenic Kotalahti Ni Belt mafic-ultramafic intrusions mark an EW-traverse from the northeastern fringe of the CFGC to the Archean craton margin (Makkonen & Huhma 2007; Fig. 1). The initial Nd isotope composition of eight Kotalahti-type intrusions (in total, 23 samples) from Makkonen & Huhma (2007) is shown in a Mg# vs. ε_{Ndi} plot (Fig. 21). Most of these samples are MgO-dominated cumulates but include some high-Mg# gabbros as well. They show a clear shift from radiogenic initial Nd isotope composition ($\varepsilon_{Nd} \approx +2$) of intrusions in the western part of the traverse (distal to the craton)

to unradiogenic values ($\varepsilon_{Nd} \approx -2$) in the proximity of the craton (Fig. 20). The Palojärvi leucogabbro is much more fractionated than the Kotalahti-type intrusions but still has radiogenic Nd with an initial $\varepsilon_{Nd} \approx +2.6$. The two examples of the Ti-Fe-P gabbros and associated granites (Perämaa-Honkajoki from the western part of the CFGC; Kälä-Puula from the southeastern fringe of the CFGC) are also rather fractionated, show little change in initial Nd isotope composition along fractionation state and are, with an initial ε_{Nd} of ~ 0, measurably less radiogenic than the Palojärvi-Haukkavuori assemblage. Moreover, the Ti-Fe-P gabbros and associated granites of the CFGC do not differ from each other in terms of Nd isotope composition, whereas the Haukkajärvi granite is marginally less unradiogenic than the Palojärvi leucogabbro (initial ε_{Nd} +1.5 vs. +2.6). The studied samples being clearly more radiogenic than the Ti-Fe-P gabbros of the CFGC might point to slightly more juvenile mantle source region underneath south-central CFGC, compared to the western and southeastern fringes of it. A difference in mantle source region was also considered a possibility for the shift in the ε_{Nd} values of the Kotalahti Ni Belt, even though the spatial change in the ε_{Nd} values (Fig. 21) could also be the result of increased contamination of the mafic-ultramafic magmas with Archean (unradiogenic) Nd from cratonic crust during fractionation (cf. Makkonen & Huhma 2007). The high ε_{Nd} in the studied samples indicate a lack of significant crustal contamination.

5.5. Petrogenesis

5.5.1. Palojärvi

Based on the results and discussion in the previous chapters, it is clear that Palojärvi and Matokulma intrusions evolved differently. In Palojärvi, the depletion of Cr and Ni is even more pronounced indicating longer evolution history if similar parental magma is assumed.

The most primitive, least altered samples are composed of cumulus olivine or pyroxenes and plagioclase, enclosed in large, poikilitic amphibole, orthopyroxene or biotite. The parental magma calculations based on the cumulus olivine and enclosing orthopyroxene show that the concentration of MgO in the magma was low (2–4 wt.% MgO). Magmatic, poikilitic amphibole and, to lesser extent, biotite are common in Palojärvi intrusion, which indicates that the magma was hydrous.

Palojärvi intrusion fractionated from an evolved, tholeiitic basalt magma, which further evolved under low fO_2, which prevented Fe-Ti-oxides from precipitating deeper in the crust and led to the enrichment of Fe in the tholeiitic trend (e.g., Irvine & Baragar 1971, Fig. 19a). In a closed system, the fractional crystallization of olivine and plagioclase will raise the relative fO_2 in the melt as Fe^{2+} is preferentially incorporated into olivine (Snyder et al. 1993). This rise of oxygen fugacity triggered crystallisation of ilmenomagnetite which causes the strong positive magnetic anomaly of the intrusion (Fig. 3).

Mixing and mingling textures and unclear cutting relations between felsic and mafic rocks seen on many observation points in Palojärvi indicate possible immiscibility between the two magma types. These textures could be the result of back veining of the country rock or may register bimodal magmatism. The latter has been described from the nearby Kaipola layered intrusion, which also displays geochemical and mineralogical similarity with the Palojärvi intrusion (Fig. 19; Nironen et al. 2000, Peltonen 2005).

5.5.2. Matokulma

Olivine is absent in the Matokulma gabbros, despite being a normative mineral in all samples and typically the first liquidus phase in both MORB and arc-type basalts (e.g., Sisson & Grove 1993, Arculus 2004; Schmidt & Jagouz 2017). Although absent in the studied samples, olivine ± spinel may have fractionated earlier during the evolution of the magma and decreased the

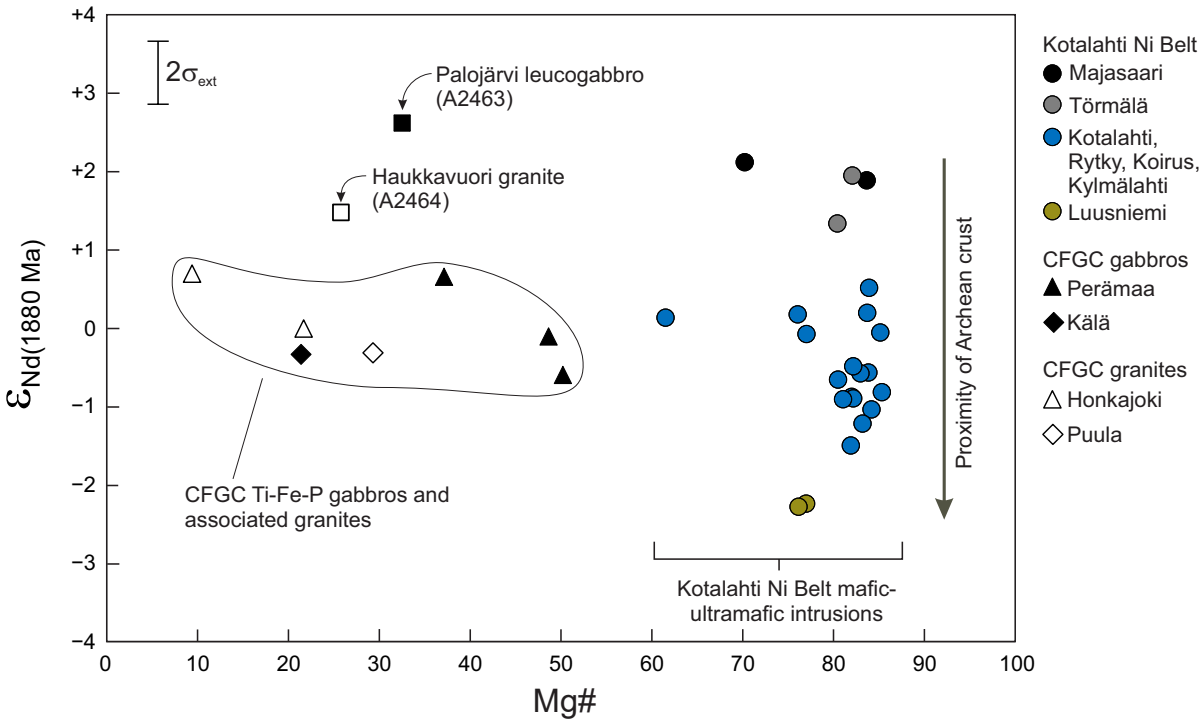

Figure 21. Mg# versus_εNdi. Initial Nd isotope composition of the studied samples, Kotalahti-type mafic-ultramafic intrusions and Ti-Fe-P gabbros and associated granites from the CFGC area, plotted against Mg# [molar 100*MgO/(MgO + 0.85*FeO_{tot})]. Legend labels point to intrusions in the reference data. External 2σ error of the initial ε_{Nd} values (±0.4 ε) is indicated. Reference data from Makkonen & Huhma (2007), Nironen et al. (2000), Rämö (1986), and Rämö et al. (2001).

concentration of MgO and increased the SiO_2 in the evolving magma (Nicholls & Ringwood 1972; Straub et al. 2008). The increasing silica decreases the solubility of sulphur which would eventually cause the formation of a sulphide melt (e.g., Ripley & Li 2013) depleting the melt of PGEs due to the extremely high partition coefficients of these elements to the sulphide melt (Naldrett 1999; Cawthorn et al. 2005). The orthopyroxene present in numerous samples could have been formed by peritectic reactions between olivine and the residual melt (Müntener et al. 2001; Hamada & Fujii 2008; Straub et al. 2008, Dessimoz et al. 2012), crystallization from a basaltic magma that assimilates silica (Ripley & Li 2013) or from hydrous basaltic magmas with P > 0.4 MPa (Hamada & Fujii 2008). These reactions would, however, result in high Mg# and Ni concentration in orthopyroxene, which is not observed in Matokulma. The crystallization of forsterite would efficiently reduce the MgO and Ni content of the magma and increase all the other components not incorporated into olivine. The fractionation and accumulation of olivine would also reduce the density of the residual magma and allow it to ascend in the crust (e.g., Gust & Perfit 1987). Clinopyroxene fractionation followed and further depleted the magma of MgO and started the decrease of Cr, together with the crystallization of accessory chromite.

Based on the lack of iron enrichment and Fe-Ti oxides in addition to the low magnetic susceptibility of the Matokulma gabbro, magnetite fractionation probably happened earlier. The depletion of MgO and enrichment of SiO_2 move the magma composition towards more evolved, basaltic andesite to andesitic compositions, where orthopyroxene is stabilized as the liquidus phase

after clinopyroxene (Pichavant & Macdonald 2007). Orthopyroxene may also be stabilized by the assimilation of silica (Ripley & Li 2013). In the pyroxene-hornblendite sample (SIKA-2017-115.2), orthopyroxene and clinopyroxene are euhedral cumulus phases. Some of the clinopyroxene were transported to the current erosional level where they were in disequilibrium with the magma forming peritectic interstitial magmatic amphibole (e.g., Marxer et al. 2023), as indicated by the high Cr concentration of amphiboles surrounding cumulus clinopyroxene (Conrad & Kay 1984). The evolution of the magma took place in relatively high fO_2, based on the modest enrichment of iron and the liquid line of descent from the tholeiitic, magnesium-rich gabbros to the mostly calc-alkaline dike rocks. The shift from tholeiitic to calc-alkaline compositions from the gabbros to the dikes may have been caused by high concentration of water in the residual magma (Grove et al. 2003).

Based on similarities in geochemistry and mineralogy, the dike rocks intruding the country rocks are comagmatic with the gabbros and probably represent late residual magma fractions, as exhibited by the enrichment in trace element concentrations (Fig. 14). The trace element characteristics imply that the parental melt was an evolved, basalt or a basaltic andesite, with arc-type trace element enrichment and depletion patterns, related to the alteration by volatiles released by dehydration reactions in the subducting slab (LILE enrichment, HFSE depletion). The presence of ubiquitous, oikocrystic amphibole implies that the magma was hydrous and reached amphibole saturation with progressive fractionation.

6. Conclusions

The studied gabbro intrusions were formed from fractionated tholeiitic basalt or basaltic andesite magmas that, based on the presence of late-magmatic amphibole, were hydrous. The trace element patterns indicate a source metasomatised by subduction-related fluids.

Matokulma and Palojärvi intrusions did not crystallise from primary, mantle-derived melts, as the estimated MgO_{liq} contents were only approximately 4–6 wt.% and 2–4wt.% MgO, respectively. Based on the higher concentration of MgO, Cr, and Ni in whole-rock and mineral chemistry, the Matokulma intrusion is less fractionated than Palojärvi, which is more enriched in Fe and Ti.

The studied intrusions show similarities to the known Ni-Cu mineralized Vammala and Kotalahti type intrusions in trace element chemistry patterns and in the presence of magmatic interstitial amphibole, but they are more evolved. The high ε_{Nd} of the studied Palojärvi samples also indicates a lack of significant crustal contamination, an important process to achieve sulphide saturation, that took place in mineralized intrusions both in Vammala and Kotalahti. Furthermore, due to the evolved nature of the studied intrusions, they have low potential for Ni-Cu-PGE mineralizations. The layered Palojärvi intrusion could theoretically host a Fe-Ti-V mineralization deeper in the stratigraphy, based on the presence of vanadiferous ilmenomagnetite.

The zircon U-Pb age from Palojärvi (1882 ± 5 Ma) Ma suggests that the intrusion was formed during the main stage of the Svecofennian mafic-ultramafic magmatism, ca. 1.88 Ga. The initial Nd isotope composition of the Palojärvi leucogabbro is, despite the vast difference in fractionation state, comparable to that of synorogenic mafic-ultramafic intrusions of Kotalahti-type intrusions farther to the northeast and may indicate a juvenile domain in the mantle underneath south-central CFGC.

Acknowledgements

We acknowledge Jarmo Kohonen, Jussi Heinonen, Tapio Halkoaho, and Shenghong Yang for their comments and suggestions that improved this paper. We acknowledge Antti Mäkelä's invaluable help in sampling, Hugh O'Brien and the late Yann

Lahaye for instrument tuning and spreadsheet for data reduction, Sari Lukkari for SEM images, Leena Järvinen and Lasse Heikkinen for zircon hand picking and mount preparation, Seppo Töllikkö and Niko Turunen for crushing and mineral separation, and Lassi Pakkanen for mineral chemistry. Petri Peltonen is thanked for providing the Vammala and Kaipola whole-rock chemical data.

Authorship contribution statement

S.K. — Fieldwork and sampling, analytical work, data analysis and interpretation, modelling, writing, visualization; H.V.M. — Background, data analysis and interpretation, modelling, writing and editing; P.M. — Background, data analysis and interpretation, visualization, writing and editing; O.T.R. — Background, data analysis and interpretation, visualization, writing and editing; H.H. — Analytical work, data analysis and interpretation; M.N. — Modelling, data analysis and interpretation, visualization.

Supplementary data

Electronic Appendices A–C for this article are available via Bulletin of the Geological Society of Finland web page.

References

Arculus, R.J., 2004. Evolution of arc magmas and their volatiles. Geophysical Monograph Series 150, 95–108. https://doi.org/10.1029/150GM09

Akiander, K.V., 1972. Titaanirautamalmitutkimukset Keski-Pohjanmaalla. Rautaruukki Oy, Archive report OU 22/72, 3 p., 5 app.

Barnes, S.J., Makkonen, H.V., Dowling, S.E., Hill, R.E.T. & Peltonen, P., 2009. The 1.88 Ga Kotalahti and Vammala nickel belts, Finland: Geochemistry of the mafic and ultramafic metavolcanic rocks. Bulletin of the Geological Society of Finland 81, 103–141. https://doi.org/10.17741/bgsf/81.2.002

Bedrock of Finland – DigiKP. Digital map database (Electronic resource). Geological Survey of Finland, Espoo (referred 31.08.2021). Version 2.0.

Bender, J.F., Hodges, F.N. & Bence, A.E., 1978. Petrogenesis of basalts from the project FAMOUS area: experimental study from 0 to 15 kbars. Earth and Planetary Science Letters 41, 277–302. https://doi.org/10.1016/0012-821X(78)90184-X

Cawthorn, G.R., Barnes, S.J., Ballhaus, C. & Malitch, K.N., 2005. Platinum Group Element, Chromium, and Vanadium Deposits in Mafic and Ultramafic Rocks. In Hedenquist, J.W., Thompson, J.H.F., Goldfarb, R.J., Richards, J.P. One Hundredth Anniversary Volume, Society of Economic Geologists. https://doi.org/10.5382/AV100.09

Claesson, S., Huhma, H., Kinny, P. D. & Williams, I. S., 1993. Svecofennian detrital zircon ages—implications for the Precambrian evolution of the Baltic Shield. Precambrian Research 64, 109–130. https://doi.org/10.1016/0301-9268(93)90071-9

Claeson, D. T. & Meurer, W. P., 2004. Fractional crystallization of hydrous basaltic "arc-type" magmas and the formation of amphibole-bearing gabbroic cumulates. Contributions to Mineralogy and Petrology 147, 288–304. https://doi.org/10.1007/s00410-003-0536-0

Conrad, W.K. & Kay, R.W., 1984. Ultramafic and Mafic Inclusions from Adak Island: Crystallization History, and Implications for the Nature of Primary Magmas and Crustal Evolution in the Aleutian Arc. Journal of Petrology 25, 88–125. https://doi.org/10.1093/petrology/25.1.88

DeBari, S.M. & Coleman, R.G., 1989. Examination of the deep levels of an island arc: Evidence from the Tonsina ultramafic-mafic assemblage, Tonsina, Alaska. Journal of Geophysical Research: Solid Earth 94, 4373–4391. https://doi.org/10.1029/JB094iB04p04373

Dessimoz, M., Müntener, O. & Ulmer, P., 2012. A case for hornblende dominated fractionation of arc magmas: the Chelan Complex (Washington Cascades). Contributions to Mineralogy and Petrology 163, 567–589. https://doi.org/10.1007/s00410-011-0685-5

Duchesne, J. C., Shumlyanskyy, L. & Charlier, B., 2006. The Fedorivka layered intrusion (Korosten Pluton, Ukraine): an example of highly differentiated ferrobasaltic evolution. Lithos 89, 353–376. https://doi.org/10.1016/j.lithos.2006.01.003

Elthon, D., Casey, J.F. & Komor, S., 1982. Mineral chemistry of ultramafic cumulates from the North Arm Mountain Massif of the Bay of Islands ophiolite: Evidence for high-pressure crystal fractionation of oceanic basalts. Journal of Geophysical Research: Solid Earth 87, 8717–8734. https://doi.org/10.1029/JB087iB10p08717

Falloon, T.J. & Green D.H., 1987. Anhydrous Partial Melting of MORB Pyrolite and Other Peridotite Compositions at 10kbar: Implications for the Origin of Primitive MORB Glasses. Mineralogy and Petrology 37, 181–219. https://doi.org/10.1007/BF01161817

Gaetani, G. A. & Grove, T. L., 1998. The influence of water on melting of mantle peridotite. Contributions to Mineralogy and Petrology 131, 323-346. https://doi.org/10.1007/s004100050396

Green, D.H., Edgar, A.D., Beasley, P., Kiss, E. & Ware, N.G., 1974. Upper mantle source for some hawaiites, mugearites and benmoreites, Contributions to Mineralogy and Petrology 48, 33–43. https://doi.org/10.1007/BF00399108

Grove, T.L., Elkins-Tanton, L.T., Parman, S.W., Chatterjee, N., Muntener, O. & Gaetani, G. A., 2003. Fractional crystallization and mantle-melting controls on calc-alkaline differentiation trends. Contributions to Mineralogy and Petrology 145, 515–533. https://doi.org/10.1007/s00410-003-0448-z

Gust, D.A. & Perfit, M.R., 1987. Phase relations of a high-Mg basalt from the Aleutian island arc: implications for primary island arc basalts and high-Al basalts. Contributions to Mineralogy and Petrology 97, 7–18. https://doi.org/10.1007/BF00375210

Hamada, M. & Fujii, T. 2008. Experimental constraints on the effects of pressure and H_2O on the fractional crystallization of high-Mg island arc basalt. Contributions to Mineralogy and Petrology 155, 767–790. https://doi.org/10.1007/s00410-007-0269-6

Häkli, T.A., 1971. Silicate nickel and its application to the exploration of nickel ores. Bulletin of the Geological Society of Finland 43, 247–263. https://doi.org/10.17741/bgsf/43.2.009

Hawthorne, F. C., Oberti, R., Harlow, G. E., Maresch, W. V., Martin, R. F., Schumacher, J. C., Welch, M. D. 2012. Nomenclature of the amphibole supergroup. American Mineralogist 97, 2031-2048. https://doi.org/10.2138/am.2012.4276

Heikura, A. 2017. The volcanic rocks of the Länkipohja-Jämsä area in the southern part of the Central Finland Granitoid Complex. MSc thesis, University of Oulu, Oulu Mining School, Finland, 81 p. Available online: https://tupa.gtk.fi/opinnayte/heikura_antti_gradu.pdf

Herzberg, C. & O'Hara, M.J., 2002. Plume-Associated Ultramafic Magmas of Phanerozoic Age. Journal of Petrology 43, 1857–1883. https://doi.org/10.1093/petrology/43.10.1857

Huhma, H., Kousa, J. & Luukas, J., 2021. Geochronology of the Paleoproterozoic Pyhäsalmi-Vihanti district, central Finland. Geological Survey of Finland, Open File Research Report 8/2021

Irvine, T.N.J. & Baragar, W.R.A., 1971. A guide to the chemical classification of the common volcanic rocks. Canadian Journal of Earth Sciences 8, 523–548. https://doi.org/10.1139/e71-055

Kelley, K.A. & Cottrell, E., 2009. Water and the Oxidation State of Subduction Zone Magmas. Science 325, 605–607. https://doi.org/10.1126/science.1174156

Klemme, S., Günther, D., Hametner, K., Prowatke, S. & Zack, T., 2006. The partitioning of trace elements between ilmenite, ulvospinel, armalcolite and silicate melts with implications for the early differentiation of the moon. Chemical Geology 234, 251–263. https://doi.org/10.1016/j.chemgeo.2006.05.005

Kähkönen, Y. 1989. Geochemistry and petrology of the metavolcanic rocks of the early Proterozoic Tampere Schist Belt, southern Finland. In: Kähkönen, Y. Geochemistry and petrology of the metavolcanic rocks of the early Proterozoic Tampere Schist Belt, southern Finland. Geological Survey of Finland, Bulletin 345, 1–104. Available online: https://tupa.gtk.fi/julkaisu/bulletin/bt_345.pdf

Kärkkäinen, N.K. & Bornhorst, T.J., 2003. The Svecofennian gabbro-hosted Koivusaarenneva magmatic ilmenite deposit, Kälviä, Finland. Mineralium Deposita 38, 169–184. https://doi.org/10.1007/s00126-002-0297-0

Karvinen, S., 2019. Geochemistry and Petrology of the Matokulma, Palojärvi, and Hongonniittu Gabbro intrusions, Central Finland Granitoid Complex. MSc Thesis, University of Helsinki, Department of Geosciences and Geography, Finland, 111 p. Available online: https://hdl.handle.net/10138/307318

Lahtinen, R., Huhma, H., Sipilä, P. & Vaarma, M., 2017. Geochemistry, U-Pb geochronology and Sm-Nd data from the Paleoproterozoic Western Finland supersuite – A key component in the coupled Bothnian oroclines. Precambrian Research 299, 264–281. https://doi.org/10.1016/j.precamres.2017.07.025

Laiti, I.O. 1976. Mänttä. Geological Map of Finland 1:100 000, Pre-Quaternary Rocks, Sheet 2231. Geological Survey of Finland.

Lamberg, P. 2005. From genetic concepts to practice - lithogeochemical identification of Ni-Cu mineralised intrusions and localisation of the ore. Geological Survey of Finland, Bulletin 402, 264 p. Available online: https://tupa.gtk.fi/julkaisu/bulletin/bt_402.pdf

Locock A. J. 2014. An Excel spreadsheet to classify chemical analyses of amphiboles following the IMA 2012 recommendations. Computers and Geosciences 62, 1-11. https://doi.org/10.1016/j.cageo.2013.09.011

Makkonen, H.V. 1996. 1.9 Ga tholeiitic magmatism and related Ni-Cu deposition in the Juva area, SE Finland. Geological Survey of Finland, Bulletin 386, 101 pp. Available online: https://tupa.gtk.fi/julkaisu/bulletin/bt_386.pdf

Makkonen, H.V. 2015. Nickel Deposits of the 1.88 Ga Kotalahti and Vammala Belts. In: Maier, W.D., Lahtinen, R., O'Brien, H. (Eds.), Mineral Deposits of Finland. Elsevier, pp. 253–290. https://doi.org/10.1016/B978-0-12-410438-9.00010-8

Makkonen, H.V. & Huhma, H., 2007. Sm-Nd data for mafic-ultramafic intrusions in the Svecofennian (1.88 Ga) Kotalahti Nickel Belt, Finland - Implications for crustal contamination at the Archaean/Proterozoic boundary. Bulletin of the Geological Society of Finland 79, 175–201. https://doi.org/10.17741/bgsf/79.2.003

Makkonen, H. V., Mäkinen, J. & Kontoniemi, O., 2008. Geochemical discrimination between barren and mineralized intrusions in the Svecofennian (1.9 Ga) Kotalahti Nickel Belt, Finland. Ore Geology Reviews *33*, 101–114. https://doi.org/10.1016/j.oregeorev.2006.05.011

Makkonen, H.V., Halkoaho, T., Konnunaho, J., Rasilainen, K., Kontinen, A. & Eilu, P., 2017. Ni-(Cu-PGE) deposits in Finland – Geology and exploration potential. Ore Geology Reviews 90, 667–696. https://doi.org/10.1016/j.oregeorev.2017.06.008

Marxer, F., Ulmer, P. & Müntener, O., 2023. Ascent-driven differentiation: a mechanism to keep arc magmas metaluminous? Contributions to Mineralogy and Petrology 178. https://doi.org/10.1007/s00410-023-02035-7

McDonough, W.F. & Sun, S.S., 1995. The composition of the Earth. Chemical geology 120, 223–253. https://doi.org/10.1016/0009-2541(94)00140-4

Mikkola, P., Heilimo, E., Luukas, J., Kousa, J., Aatos, S., Makkonen, H., Niemi, S., Nousiainen, M., Ahven, M., Romu, I. & Hokka, J., 2018b. Geological evolution and structure along the southeastern border of the Central Finland Granitoid Complex. In: Mikkola, P., Hölttä, P., Käpyaho, A. (Eds.) Development of the Paleoproterozoic Svecofennian orogeny: new constraints from the southeastern boundary of the Central Finland Granitoid Complex. Geological Survey of Finland, Bulletin 407, 5–27. https://doi.org/10.30440/bt407.1

Mikkola, P., Mönkäre, K., Ahven, M. & Huhma, H., 2018a. Geochemistry and age of the Paleoproterozoic Makkola suite volcanic rocks in central Finland. In: Mikkola, P., Hölttä, P., Käpyaho, A. (Eds.) Development of the Paleoproterozoic Svecofennian orogeny: new constraints from the southeastern boundary of the Central Finland Granitoid Complex. Geological Survey of Finland, Bulletin 407, 85–105. https://doi.org/10.30440/bt407.5

Molnár, F., Middleton, A., Stein, H., O'Brien, H., Lahaye, Y., Huhma, H., Pakkanen, L. & Johanson, B., 2018. Repeated syn- and post-orogenic gold mineralization events between 1.92 and 1.76 Ga along the Kiistala Shear Zone in the Central Lapland Greenstone Belt, northern Finland. Ore Geology Reviews, 936–956. https://doi.org/10.1016/j.oregeorev.2018.08.015

Morimoto, N., Fabries, J., Ferguson, A.K., Ginzburg, I.V., Ross, M., Seifert, F.A. & Zussman, J., 1988. Nomenclature of pyroxenes. American Mineralogist 73, 1123–1133

Müntener, O., Kelemen, P.B. & Grove, T.L., 2001. The role of H_2O during crystallization of primitive arc magmas under uppermost mantle conditions and genesis of igneous pyroxenites: an experimental study. Contributions to Mineralogy and Petrology 141, 643–658. https://doi.org/10.1007/s004100100266

Naldrett, A.J., 1999. World-class Ni-Cu-PGE deposits: key factors in their genesis. Mineralium Deposita 34, 227–240. https://doi.org/10.1007/s001260050200

Nicholls, I.A. & Ringwood, A.E., 1972. Production of silica-saturated tholeiitic magmas in island arcs. Earth and Planetary Science Letters 17, 243–246. https://doi.org/10.1016/0012-821X(72)90282-8

Nikkilä, K., Mänttäri, I., Nironen, M., Eklund, O. & Korja, A., 2016. Three stages to form a large batholith after terrane accretion – An example from the Svecofennian orogen. Precambrian Research 281, 618–638. https://doi.org/10.1016/j.precamres.2016.06.018

Nironen, M. 1989. Emplacement and structural setting of granitoids in the early Proterozoic Tampere and Savo Schist Belts, Finland - implications for contrasting crustal evolution. Geological Survey of Finland, Bulletin 346, 83 p. Available online: http://tupa.gtk.fi/julkaisu/bulletin/bt_346.pdf

Nironen, M. 2017. Guide to the Geological Map of Finland – Bedrock 1:1 000 000. In: Nironen, M. (ed.) Bedrock of Finland at the scale 1:1 000 000 - Major stratigraphic units, metamorphism and tectonic evolution. Geological Survey of Finland, Special Paper 60, 41–76. Available online: https://tupa.gtk.fi/julkaisu/specialpaper/sp_060.pdf

Nironen, M., Elliott, B.A. & Rämö, O.T., 2000. 1.88–1.87 Ga post-kinematic intrusions of the Central Finland Granitoid Complex: a shift from C-type to A-type magmatism during lithospheric convergence. Lithos 53, 37–58. https://doi.org/10.1016/S0024-4937(00)00007-4

Nironen, M., Kousa, J., Luukas, J. & Lahtinen, R., 2016. Geological Map of Finland – Bedrock 1:1 000 000. Geological Survey of Finland.

Pearce, T.H. 1968. A contribution to the theory of variation diagrams. Contributions to Mineralogy and Petrology, 19, 142–157. https://doi.org/10.1007/BF00635485

Peltonen, P., 1995a. Petrogenesis of ultramafic rocks in the Vammala Nickel Belt: Implications for crustal evolution of the early Proterozoic Svecofennian arc terrane. Lithos 34, 253–274. https://doi.org/10.1016/0024-4937(94)00042-Z

Peltonen, P., 1995b. Magma-country rock interaction and the genesis of Ni-Cu deposits in the Vammala Nickel Belt, SW Finland. Mineralogy and Petrology 52, 1–24. https://doi.org/10.1007/BF01163124

Peltonen, P. & Elo, S., 1999. Petrology of the Kaipola layered intrusion, southern Finland. Geological Survey of Finland, Special Paper 27, 21–24.

Peltonen, P. 2005. Mafic-Ultramafic intrusions of the Svecofennian orogen. In: Lehtinen, M., Nurmi, P.A., Rämö, O.T. (Eds.). The Precambrian Geology of Finland – Key to the Evolution of the Fennoscandian Shield. Elsevier B.V., Amsterdam, pp. 413–447. https://doi.org/10.1016/S0166-2635(05)80010-6

Pichavant, M. & Macdonald, R., 2007. Crystallization of primitive basaltic magmas at crustal pressures and genesis of the calc-alkaline igneous suite: experimental evidence from St Vincent, Lesser Antilles arc. Contributions to

Mineralogy and Petrology 154, 535–558. https://doi.org/10.1007/s00410-007-0208-6

Powell, M., 1978. Crystallisation conditions of low-pressure cumulate nodules from the Lesser Antilles island arc. Earth and Planetary Science Letters 39, 162–172. https://doi.org/10.1016/0012-821X(78)90152-8

Putirka, K.D. 2008. Thermometers and Barometers for Volcanic Systems. Reviews in Mineralogy & Geochemistry, 69, 61–120. https://dx.doi.org/10.1515/9781501508486-004

Rämö, T. 1986. Honkajoen Perämaan emäksinen intruusio – erityisesti sen gabro-osien petrografia, mineralogia ja petrologia. MSc. thesis, University of Helsinki, Finland. (in Finnish)

Rämö, O.T., Vaasjoki, M., Mänttäri, I., Elliott, B.A. & Nironen, M., 2001. Petrogenesis of the post-kinematic magmatism of the Central Finland Granitoid Complex I; radiogenic isotope constraints and implications for crustal evolution. Journal of Petrology 42, 1971–1993. https://doi.org/10.1093/petrology/42.11.1971

Rasilainen, K., Lahtinen, R. & Bornhorst, T. J., 2007. The Rock Geochemical Database of Finland Manual. Geological Survey of Finland, Report of Investigation 164, 38 p. Available online: https://tupa.gtk.fi/julkaisu/tutkimusraportti/tr_164.pdf

Reynolds, I.M. 1985. The nature and origin of titaniferous magnetite-rich layers in the upper zone of the Bushveld Complex; a review and synthesis. Economic Geology 80, 1089–1108. https://doi.org/10.2113/gsecongeo.80.4.1089

Ripley, E.M. & Li, C., 2013. Sulfide saturation in mafic magmas: Is external sulfur required for magmatic Ni-Cu-(PGE) ore genesis? Economic geology 108, 45–58. https://doi.org/10.2113/econgeo.108.1.45

Roeder, P.L. & Emslie, R.F., 1970. Olivine-liquid equilibrium. Contributions to Mineralogy and Petrology 29, 275–289. https://doi.org/10.1007/BF00371276

Roeder, P.L., 1974. Activity of iron and olivine solubility in basaltic liquids. Earth and Planetary Science Letters 23, 397–410. https://doi.org/10.1016/0012-821X(74)90129-0

Schmidt, M. W., & Jagoutz, O., 2017. The global systematics of primitive arc melts. Geochemistry, Geophysics, Geosystems 18, 2817–2854. https://doi.org/10.1002/2016GC006699Sisson, T.W. & Grove, T L., 1993. Temperatures and H_2O contents of low-MgO high-alumina basalts. Contributions to Mineralogy and Petrology 113, 167–184. https://doi.org/10.1007/BF00283226

Sjöblom, B. 1990. Mäntän kartta-alueen kallioperä. Summary Pre-Quaternary rocks of the Mänttä map sheet area. Geological Map of Finland 1:100 000, Explanation to the Maps of Pre-Quaternary Rocks, Sheet 2231. Geological Survey of Finland. 64 p.

Snyder, D., Carmichael, I.S. & Wiebe, R.A., 1993. Experimental study of liquid evolution in an Fe-rich, layered mafic intrusion: constraints of Fe-Ti oxide precipitation on the T-fO2 and T-ρ paths of tholeiitic magmas. Contributions to Mineralogy and Petrology 113, 73–86. https://doi.org/10.1007/BF00320832

Straub, S.M., LaGatta, A.B., Martin-Del Pozzo, A.L. & Langmuir, C.H. 2008. Evidence from high-Ni olivines for a hybridized peridotite/pyroxenite source for orogenic andesites from the central Mexican Volcanic Belt. Geochemistry, Geophysics, Geosystems 9. https://doi.org/10.1029/2007GC001583

Sun, S.S. & McDonough, W.F., 1989. Chemical and isotopic systematics of oceanic basalts: implications for mantle composition and processes. Geological society, London, Special Publications 42, 313–345. https://doi.org/10.1144/GSL.SP.1989.042.01.19

Toplis, M.J. 2005. The thermodynamics of iron and magnesium partitioning between olivine and liquid: criteria for assessing and predicting equilibrium in natural and experimental systems. Contributions to Mineralogy and Petrology 149, 22–39. https://doi.org/10.1007/s00410-004-0629-4

Toplis, M.J. & Corgne, A., 2002. An experimental study of element partitioning between magnetite, clinopyroxene and iron-bearing silicate liquids with particular emphasis on vanadium. Contributions to Mineralogy and Petrology 144, 22–37. https://doi.org/10.1007/s00410-002-0382-5

Villiger, S., Ulmer, P. & Müntener, O., 2007. Equilibrium and fractional crystallization experiments at 0.7 GPa; the effect of pressure on phase relations and liquid compositions of tholeiitic magmas. Journal of Petrology 48, 159–184. https://doi.org/10.1093/petrology/egl058

Vincent, E. A. & Phillips, R., 1954. Iron-Titanium oxide minerals in layered gabbros of the Skaergaard intrusion, East Greenland: Part I. Chemistry and ore-microscopy. Geochimica et Cosmochimica Acta 6, 1–26. https://doi.org/10.1016/0016-7037(54)90026-5

Woodhead, J., Eggins, S. & Gamble, J., 1993. High field strength and transition element systematics in island arc and back-arc basin basalts: Evidence for multi-phase melt extraction and a depleted mantle wedge. Earth and Planetary Science Letters 114, 491–504. https://doi.org/10.1016/0012-821X(93)90078-N